
Research Article: New Research | Development

Common origin of the cerebellar dual somatotopic areas revealed by tracking embryonic Purkinje cell clusters with birthdate tagging

<https://doi.org/10.1523/ENEURO.0251-20.2020>

Cite as: eNeuro 2020; 10.1523/ENEURO.0251-20.2020

Received: 12 June 2020

Revised: 29 September 2020

Accepted: 30 September 2020

This Early Release article has been peer-reviewed and accepted, but has not been through the composition and copyediting processes. The final version may differ slightly in style or formatting and will contain links to any extended data.

Alerts: Sign up at www.eneuro.org/alerts to receive customized email alerts when the fully formatted version of this article is published.

Copyright © 2020 Tran-Anh et al.

This is an open-access article distributed under the terms of the Creative Commons Attribution 4.0 International license, which permits unrestricted use, distribution and reproduction in any medium provided that the original work is properly attributed.

1 **Common origin of the cerebellar dual**
2 **somatotopic areas revealed by tracking**
3 **embryonic Purkinje cell clusters with**
4 **birthdate tagging**

5

6 Abbreviated title:

7 Embryonic Purkinje cell compartmentalization

8

9 Khoa Tran-Anh^a, Jingyun Zhang^a, Viet Tuan Nguyen-Minh^a, Hirofumi Fujita^{a,c}, Tatsumi
10 Hirata^d and Izumi Sugihara^{a,b}

11

12 ^aDepartment of Systems Neurophysiology, Graduate School of Medical and Dental
13 Sciences and ^bCenter for Brain Integration Research, Tokyo Medical and Dental
14 University, 1-5-45 Yushima, Bunkyo-ku, Tokyo 113-8519, Japan

15 ^cDepartment of Otolaryngology-Head and Neck Surgery, Johns Hopkins University,
16 School of Medicine, 720 Rutland Avenue, Baltimore, Maryland 21205, U.S.A.

17 ^dBrain Function Lab, National Institute of Genetics, Yata, Mishima-shi, Shizuoka-ken
18 411-8540, Japan

19

20 **Corresponding author:** Dr. Izumi Sugihara

21 Email: isugihara.phy1@tmd.ac.jp

22 **Number of pages:** 31

23 **Number of figures:** 10, tables: 5

24 **Competing interests**

25 Authors have no competing interests to declare.

26 **Acknowledgments**

27 This study was supported by Grant-in-Aid for Scientific Research (KAKENHI) from
28 the Japan Society for the Promotion of Science (19K06919 to I.S., 20H03345 to T.H.)
29 and ROIS Challenging Exploratory Research Projects for the Future Grant to T.H. The

30 authors thank Dr. Gideon Sarpong and Mr. Richard Nana Abankwah Owusu Mensah for
31 proofreading the manuscript. The authors thank Dr. Yuichi Ono of KAN Research
32 Institute Inc. for providing us with anti-Corl2 antibody.

33 **Author contributions:** K.T.-A., J.Z., V.T.N.-M., H.F., T.H. and I.S. performed research;
34 K.T.-A., J.Z., V.T.N.-M., H.F. and I.S. analyzed data; K.T.-A., H.F. and I.S. edited the
35 paper; K.T.-A., H.F. and I.S. designed research; K.T.-A., H.F. and I.S. wrote the paper.

36

37

38 **Abstract**

39 One of the notable characteristics of the functional localization in the cerebellar
40 cortex is the dual representation of the body (somatotopy) along with its
41 anterior-posterior axis. This somatotopy is conspicuous in the C1/C3 module, which is
42 demarcated as the multiple zebrin-negative and weakly-positive stripes in dual
43 paravermal areas in anterior and posterior lobules within the cerebellar compartments.
44 In this report, we describe the early formation process of the cerebellar
45 compartmentalization, particularly in the C1/C3 module. As developing PCs guide
46 formation of the module-specific proper neuronal circuits in the cerebellum, we
47 hypothesized that the rearrangement of embryonic Purkinje cell (PC) clusters shapes the
48 adult cerebellar compartmentalization. By identifying PC clusters with immunostaining
49 of marker molecules and genetical birthdate-tagging with *Neurog2-CreER (G2A)* mice,
50 we clarified the three-dimensional spatial organization of the PC clusters and tracked
51 the lineage relationships among the PC clusters from embryonic day 14.5 (E14.5) till
52 E17.5. The number of recognized clusters increased from 9 at E14.5 to 37 at E17.5.
53 Among E14.5 PC clusters, the c-l (central-lateral) cluster which lacked E10.5-born PCs
54 divided into five c-l lineage clusters. They separately migrated underneath other clusters
55 and positioned far apart mediolaterally as well as rostrocaudally by E17.5. They were
56 eventually transformed mainly into multiple separate zebrin-negative and
57 weakly-positive stripes, which together configured the adult C1/C3 module, in the
58 anterior and posterior paravermal lobules. The results indicate that the spatial
59 rearrangement of embryonic PC clusters is involved in forming the dual somatotopic
60 areas in the adult mouse paravermal cerebellar cortex.

61

62 **Significance statement**

63 Genetically programmed morphogenetic processes in the embryonic brain can
64 form a highly organized anatomical complex in the postnatal brain. The adult
65 cerebellum has a complex functional localization; one of the challenging aspects of

66 which is the dual representation of somatosensorimotor function in both the anterior and
67 posterior paravermal areas. To elucidate morphogenetic processes of the intricate
68 organization of the cerebellar cortex, we tracked lineages of early cerebellar PC clusters
69 by birthdate-tagging methods. Starting with nine clusters at embryonic day 14.5, we
70 clarified the differentiation of lineage of all clusters in later stages. Our results indicate
71 that the spatial differentiation of embryonic PC clusters is involved in forming the basic
72 cerebellar organization of the mouse brain.

73

74

75 **Introduction**

76 Representation of the somatotopy is deeply involved in the motor control
77 function in the cerebellum (Manni and Petrosini, 2004). Electrophysiological and
78 neuroimaging studies have shown dual somatotopic areas in the anterior and posterior
79 cerebellar lobules which is one of the noticeable features of the functional localization
80 of the cerebellar cortex of humans and other mammals (Fig. 1A; Thickbroom et al.,
81 2003; Manni and Petrosini, 2004).

82 Morphologically, the cerebellar cortex is organized by multiple longitudinal
83 striped subdivisions. Two types of mutually linked subdivisions, 1) modules and 2)
84 molecular compartments, have been identified. The modules have been defined by the
85 topographic connections of PC axons and climbing fiber axons (Fig. 1B; Voogd and
86 Glickstein, 1998; Apps et al., 2009; Cerminara et al., 2013; Fujita et al., 2013; Ruigrok
87 et al., 2015), whereas the molecular compartments have been defined by the
88 arrangement of Purkinje cells (PCs) that show heterogeneous expression of marker
89 molecules such as zebrin II or aldolase C (Fig. 1C; Brochu et al., 1990; Voogd et al.,
90 1998; Sugihara et al., 2004; Sillitoe and Joyner, 2007; Fujita et al., 2014). The
91 somatotopic representation is most clearly seen in the paravermal area in anterior and
92 posterior lobules, in which zebrin-negative and -faintly-positive stripes (equivalent with
93 C1/C3 module; Fig. 1B, C) occupy substantial proportions of the cerebellar cortex. Both
94 the anterior and posterior parts of this area are topographically innervated by the
95 climbing fiber axons originating from the dorsal accessory olive and project to the
96 anterior interposed nucleus (Ekerot et al., 1997; Cerminara et al., 2013; Ruigrok et al.,
97 2015; Low et al., 2018) to be involved in the control of fine body movements such as
98 grasping and limb cutaneous reflexes in the cat (Horn et al., 2010) and rat (Pijpers et al.,
99 2008). Because the C1/C3 module represents the main part of the cerebellar
100 somatotopic area as mentioned above, the anteroposterior separation of the C1/C3
101 module (Fig. 1B) may be the anatomical correlate for the anteroposterior dual

102 representation of somatotopy observed in animal and human cerebellums (Snider et al.,
103 1950; Stoodley et al., 2012; Guell et al., 2018).

104 PCs are born in the period between embryonic day 10.5 (E10.5) and E12.5 in
105 the ventricular zone (Hashimoto et al., 2003) and form the main body of the immature
106 cerebellum by E14.5 in mice (Goffinet, 1983). At E14.5, some eight heterogeneous
107 subsets of PCs are arranged in clustered compartments as observed by molecular marker
108 labeling (Vibulyaseck et al., 2017) or genetic profiling (Wizeman et al., 2019). At E17.5,
109 the number of heterogeneous populations of PCs increases to some 50, which are
110 arranged into clusters that are separated by PC-free gaps (Fig. 1E; Korneliussen, 1968;
111 Altman et al., 1985; Smeyne et al., 1991; Oberdick et al., 1993; Millen et al., 1995;
112 Larouche et al., 2006; Wilson et al., 2011; Fujita et al., 2012; Carter et al., 2018;
113 Wizeman et al., 2019). Each of the E17.5 clusters directly develops into an individual
114 adult PC stripe in the postnatal period (Fig. 1D; Sillitoe et al., 2009; Namba et al., 2011;
115 Fujita et al., 2012). Therefore, we hypothesized that the rearrangement of embryonic PC
116 clusters is essential in shaping the compartmental organization of the adult cerebellar
117 cortex which includes its modular organization and the dual somatotopic areas.
118 However, accurate spatial tracking of lineages of all E14.5 clusters would be required to
119 test this hypothesis.

120 Each striped compartment in the adult cerebellar cortex contains PCs generated
121 at particular timing (Hashimoto and Mikoshiba, 2003; Namba et al., 2013; Zhang et al.,
122 2020). Therefore, birthdate-specific labeling of PCs can be a useful technique to track
123 the cerebellar compartmentalization. The CreER-LoxP system that targets the *ascl1*
124 gene, which is transiently expressed at the time of neuronal differentiation, can label
125 neurons that are born at the time of tamoxifen injection (Sudarov et al., 2011). We used
126 a similar birthdate-tagging system (G2A mouse line, Hirata et al., 2019; Zhang et al.,
127 2020) that targets the *Neurog2* gene, which is expressed in neurons including PCs
128 (Zordan et al., 2008), when the neuronal progenitors start differentiating (Florio et al.,
129 2012).

130 By combining birthdate-specific labeling and molecular marker labeling of PCs
131 (Minaki et al., 2008; Fujita et al., 2012), we tracked the migration and division of all
132 embryonic PC clusters from E14.5 to E17.5 to clarify the spatial development of the
133 cerebellar compartmentalization. We then focused on the lineage of a particular E14.5
134 cluster, the fate of which was crucial to test the above hypothesis.

135

136 **Materials and Methods**

137 **Ethics statements**

138 Experimental protocols were approved by the Animal Care and Use Committee
139 (A2019-187A, A2018-148A, A2017-060C4) and Gene Recombination Experiment
140 Safety Committee (G2019-020A, 2017-040A, 2012-064C4) of Tokyo Medical and
141 Dental University.

142

143 **Animals**

144 Mice were bred and reared in a 12-12-hour light-dark cycled condition in the animal
145 facility of the university with freely available food and water. Wild-type embryo
146 samples were obtained by mating B6C3F1 males and females. The
147 C57BL/6N-Tg(*Neurogenin2*-CreER) mouse strain (G2A, deposited at RIKEN BDR
148 Accession No. CDB0512T-1,
149 <http://www2.clst.riken.jp/arg/TG%20mutant%20mice%20list.html>, Hirata et al., 2019)
150 has the transgene, in which CreER gene has been inserted into the downstream side of
151 the enhancer region of *neurogenin2* gene (*Neurog2*), presumptively on the Y
152 chromosome (Hirata et al., 2019). Since the CreER is expressed in differentiating PCs
153 after the last mitosis under the *Neurog2* enhancer (Florio et al., 2012), administration of
154 tamoxifen, a ligand of the estrogen receptor, produces Cre activity in cells in which
155 *Neurog2* is expressed in G2A mice. In
156 B6.Cg-Gt(ROSA)26Sor^{tm9(CAG-tdTomato)Hze}/J:C57BL/6N mice (Ai9, The Jackson
157 Laboratory, <https://www.jax.org/strain/007>), Cre activity produces a persistent tdTomato
158 expression in cells. Male heterozygous G2A mice were crossed with female
159 homozygous Ai9 mice to produce G2A::Ai9 embryos. The day when the vaginal plug
160 was detected was designated as E0.5. Tamoxifen (T5648-1G, Sigma, St. Louis, MO,
161 U.S.A.) was dissolved in corn oil (9 mmole/l, 032-17016, Wako, Wako Pure Chemical
162 Industries, Ltd., Osaka, Japan) and injected intraperitoneally (2.25 μ mole/mouse) one
163 time to the pregnant female at noon, 10, 11 or 12 days after the plug detection (at E10.5,
164 E11.5, E12.5). In AldocV mice (MGI:5620954, Fujita et al., 2014), aldolase C (zebrin
165 II) stripes are labeled by a mutated green fluorescent protein, Venus. We produced
166 double-homozygous Ai9::AldocV mice. An Ai9::AldocV double-homozygous female
167 was crossed with a G2A heterozygous male (Zhang et al., 2020). Tamoxifen was
168 injected into the pregnant female as above. E19.5 embryos were obtained by Cesarean
169 section from pregnant Ai9::AldocV double homozygous females which were sacrificed
170 beforehand by cervical dislocation. Male pups (G2A::Ai9::AldocV heterozygous hybrid
171 mice) were reared by a stepmother and perfused at postnatal day 42.

172

173 **Histological procedures**

174 Pregnant Ai9 females were anesthetized with an intramuscular injection of pentobarbital
175 sodium (0.1 mg/g body weight) and xylazine (0.005 mg/g body weight) to obtain
176 E14.5-E17.5 embryos at noon. Embryos were perfused transcardially with
177 phosphate-buffered saline (PBS, pH 7.4) with heparin sulfate (0.1%), and then with 4%
178 paraformaldehyde. The anesthetized female was sacrificed by cervical dislocation after
179 removing embryos. The embryo brains were dissected in chilled 4% paraformaldehyde
180 and kept in 4% paraformaldehyde for post-fixation and then soaked in sucrose solution
181 (30% with 0.05M phosphate buffer, pH 7.4) for two days. Among embryo samples
182 obtained from pregnant Ai9 female, ones that showed patterned red fluorescence
183 reporter expression in the brain were regarded as G2A::Ai9 heterozygous hybrid. Brain
184 samples were stored in the deep freezer until sectioning.

185 G2A::Ai9::AldocV heterozygous hybrid mice were anesthetized with an
186 intramuscular injection of an overdose of pentobarbital sodium (0.18 mg/g body weight)
187 and xylazine (0.009 mg/g body weight) at postnatal day 42. They were perfused
188 transcardially with PBS with heparin sulfate, and then with 4% paraformaldehyde. The
189 skull was kept in 4% paraformaldehyde for post-fixation overnight. The brain was
190 dissected and soaked in sucrose solution for two days. Brain samples were stored in the
191 deep freezer until sectioning.

192 Embryo G2A::Ai9 brains were coated with gelatin solution (10% gelatin, 10%
193 sucrose in 10mM phosphate buffer, pH 7.4, 32 °C). The gelatin block was hardened by
194 chilling and then soaked overnight in fixative with a high sucrose content (4%
195 paraformaldehyde, 30% sucrose in 0.05 M phosphate buffer, pH 7.4). Complete sets of
196 serial sections were cut coronally, horizontally and sagittally using freezing microtome
197 at a thickness of 40 μ m. The ventral surface of the medulla was regarded as the
198 horizontal plane. After washing in PBS and PBS with 0.12% Triton X-100 (PBST), each
199 complete set of sections was processed for immunostaining. Floating sections were
200 incubated on a shaker with a mixture of two or three primary antibodies produced in
201 different host animal species in PBST plus 2% normal donkey serum for 48 hours at 4
202 °C. Goat anti-EphA4 (R&D Systems), goat anti-FoxP2 (Everest Biotech), rabbit
203 anti-Corl2 (provided by Dr. Ono at KAN Research Institute) and rat
204 anti-OL-protocadherin (Millipore) are the primary antibodies used in the majority of
205 experiments. Rabbit anti-FoxP2 antibody (Abgent) was used in combination with the
206 goat primary antibody. The specificity of the above antibodies has been described
207 (Vibulyaseck et al., 2017). In some experiments, mouse anti-Calbindin-D28k
208 (Sigma-Aldrich) and rabbit anti-Calbindin-D28k (AnaSpec) antibodies were also used
209 (Table 1). The sections were then incubated with a mixture of appropriate two or three

210 secondary antibodies that were conjugated with fluorescent tags (Table 1). Some
211 sections were counterstained with 4', 6-diamidino-2-phenylindole dihydrochloride
212 (DAPI; 1:3,000; D212, Dojindo, Mashiki, Kumamoto, Japan). Finally, these sections
213 were mounted on glass slides, dried, coverslipped with water-soluble mounting medium
214 (CC mount, Sigma C9368-30ML).

215 Postnatal G2A::Ai9::AldocV brains were embedded in gelatin, and cut
216 coronally into serial sections at a thickness of 50 μ m. The complete sets of sections
217 were mounted on glass slides, dried, coverslipped with water-soluble mounting medium
218 (CC mount).

219

220 **Acquisition of digital images**

221 Fluorescent images were digitized using a cooled color CCD camera (AxioCam1Cm1,
222 Zeiss, Oberkochen, Germany) attached to a fluorescent microscope (AxioImager.Z2,
223 Zeiss) in 12-bit gray-scale with appropriate filter sets. To digitize a section of the
224 cerebellum, 2.5X objective and tiling function of the software to control digitizing (Zen
225 2 Pro, Zeiss) was used. Images of all serial sections of a brain were obtained with the
226 same exposure and gain parameters. Images were adjusted in contrast and brightness
227 and assembled using a software (ZEN 2 Pro, Zeiss and Photoshop 7, Adobe, San Jose,
228 CA, USA). High magnification confocal images were taken with a 63X objective lens
229 and appropriate filters and laser light sources attached to the confocal microscope (TCS
230 SP8, Leica, Wetzlar, Germany). Images were adjusted in contrast and brightness and
231 assembled using software (Las X, Leica). A combination of pseudo-colors was applied
232 to fluorescent and confocal images in figures. Photographs were assembled using
233 Photoshop and Illustrator software (Adobe). Digital enhancements were applied to
234 entire images and no manipulations were applied other than contrast or brightness.

235

236 **Three-dimensional reconstruction of Purkinje cell clusters**

237 Three-dimensional (3D) models of PC clusters were reconstructed through two steps: 1)
238 2D drawings of contours of identified PC clusters, and 2) 3D surface modeling with
239 these 2D drawings. Digital images of serial sections were placed in individual layers of
240 2D graphic software (Adobe Illustrator 10). Their positions and orientations were then
241 adjusted by superimposing them on each other while referring to landmark structures
242 such as the midline, the cerebellar surface and major labeled areas. The cerebellar
243 surface and contour of groups of Purkinje cell subsets and marker-labeled areas (i.e. PC
244 cluster) were drawn using curve tools of Illustrator in all sections. Distribution patterns
245 of PCs and PC-free gaps, and expression patterns of PC markers were systematically

246 observed in this procedure. Cerebellar nuclear areas identified by the lack of Corl2
247 signal were excluded from the reconstruction. After the identification of PC clusters, all
248 drawings in sections of coronal, horizontal and sagittal planes were imported into 3D
249 graphics software (Rhinoceros 4, Robert McNeel & Associates, Seattle, WA, USA),
250 with the z-axis position adjusted for each section. The 3D drawings of cerebellar
251 structures obtained from brain samples with different cutting orientations were matched
252 and compared with one another to identify structures. The 3D surface reconstructions
253 were made from a set of coronal section drawings by using the 'loft' command in
254 Rhinoceros (Fujita et al., 2012). Cerebellar fissures were reconstructed in the 3D space
255 from aligned drawings from sagittal sections.

256

257 **Definition of the relative position of a coronal plane within the cerebellum**

258 The relative position of a section in the whole extent of the cerebellum was defined
259 using percentages as described previously (Vibulyaseck et al., 2017). In short, the
260 position of the most caudal section of the coronal sections in which the cerebellum first
261 appeared was defined as 0%, whereas the position of the most rostral section in which
262 the cerebellum remained was defined as 100%. The position of other sections was
263 obtained by linear interpolation. In the case of horizontal sections, the most dorsal
264 section was defined as 0%, while the most ventral section in which the cerebellum
265 remained was defined as 100%.

266

267

268 **Results**

269 **Spatial organization of PC clusters in the embryonic cerebellums at E14.5, E15.5, 270 E16.5, and E17.5**

271 Although embryonic PC clusters were suggested to be the direct origin of adult
272 cerebellar compartments (Fujita et al., 2012), the development of embryonic PC clusters
273 has not been fully clarified before E17.5 except for the Pcdh10-positive areas which
274 have been tracked in our previous study (Vibulyaseck et al., 2017). In the first set of
275 experiments in the present study, we identified PC clusters in the entire cerebellum at a
276 1-day interval from E14.5 to E17.5. The distribution of PCs was analyzed by examining
277 the expression of particular molecular markers and PC-free gaps in serial coronal,
278 horizontal and sagittal sections in 22 wild-type B6C3F1 mouse embryos (E14.5, n=7;
279 E15.5, n=5, E16.5, n=5, E17.5, n=5). Expression of FoxP2 (relatively specific PC
280 marker, Fujita et al., 2012; Vibulyaseck et al., 2017), Corl2 (also known as Skor2,
281 specific PC marker, Minaki et al., 2008; Vibulyaseck et al., 2017), Pcdh10 (PC cluster

282 marker, Fujita et al., 2012; Vibulyaseck et al., 2017) and EphA4 (PC cluster marker
283 expressed in PCs and afferent axons, Fujita et al., 2012; Vibulyaseck et al., 2017) were
284 immunohistochemically revealed.

285

286 We compared the labeling pattern between left and right sides and among
287 different samples cut in coronal, horizontal and sagittal sections at each embryonic date.
288 Interindividual variations, such as those in the marker expression level, shape, size, and
289 positional relationships of clusters were small. Thus, we comprehensively identified PC
290 clusters at E15.5 (Fig. 3), and E16.5 (Fig. 4), and confirmed previously identified PC
291 clusters at E14.5 (Fig. 2) and E17.5 (Fig. 5; Fujita et al., 2012). We then reconstructed
292 identified PC clusters of E14.5, E15.5 and E16.5 cerebellums in the three-dimensional
293 space (Fig. 2I, 3H, 4J) primarily based on images of immunostaining on one side of
294 serial coronal sections. For those of E17.5, the previously published reconstruction
295 (Fujita et al., 2012) was incorporated with some revisions (see below; Fig. 5J).

296 At E14.5, nine PC clusters—termed medial, dorsal, central-medial,
297 central-lateral, mid-lateral, lateral, dorsolateral, rostradorsolateral, and ventrolateral (m,
298 d, c-m, c-l, ml, l, dl, rdl, and vl; based on Vibulyaseck et al., 2017)—were arranged in
299 column-shaped elongations in the rostrocaudal direction at various mediolateral and
300 dorsoventral levels (Fig. 2I). A previously designated Pcdh10-positive cluster, termed
301 "c" (Vibulyaseck et al., 2017), was revised here: it was divided into the central-medial
302 (c-m) and central-lateral (c-l) clusters because the expression of Corl2 was stronger in
303 the c-m than in the c-l (Fig. 2A–C). The distribution of these nine clusters was
304 remarkably consistent with that of the unbiasedly classified groups of PCs via
305 single-cell RNAseq (Wizeman et al., 2019; see Discussion). These clusters, thus, may
306 reflect fundamental molecular distinctions in PCs at E14.5.

307 The number of PC clusters increased from 9 at E14.5 (Fig. 2), to 18 at E15.5
308 (Fig. 3), and to 28 at E16.5 (Fig. 4). The number increased presumably because 1) new
309 PC-free gaps appeared inside a cluster, and/or 2) a part of a cluster changed in
310 molecular expression from the other part of the same cluster. Furthermore, some divided
311 clusters seemed to migrate separately. At E17.5, PC clusters were narrow in the
312 mediolateral direction but often extended rostrocaudally (longitudinally) across
313 immature lobules, somewhat resembling adult striped compartments, although they
314 were not yet arranged in a single layer but in multiple layers, shallow or deep from the
315 cerebellar surface (Fig. 5; Fujita et al., 2012).

316 Although E17.5 cerebellum contains 54 clusters identified with detailed
317 analyses (Fujita et al., 2012), this study focused on the more qualitative distinction of

318 clusters to facilitate analyses and simplify description. Namely, neighboring clusters that
319 had only slightly different molecular expression profiles and/or not clearly separated
320 from one another by intercalating PC-free gaps were combined. For example, our
321 cluster vp1-2 includes clusters vp1 and vp2 of Fujita et al. (2012). We combined 11 sets
322 of two or three neighboring E17.5 clusters into single clusters, resulting in a total of 37
323 clusters in place of 54. We adopted the nomenclature (Table 3) from Fujita et al. (2012)
324 to designate E17.5 clusters in the present study.

325

326

327 **Birthdate-specific labeling of PCs in the E14.5 cerebellum**

328 In the second set of experiments, we labeled PCs in the birthdate-specific way to
329 identify the lineage of PC clusters. The G2A mouse line expressed tamoxifen-inducible
330 Cre recombinase activity under the transcription control of proneural gene, neurogenin 2
331 (*Neurog2*). We crossed female Cre-reporter mice (Ai9) with male heterozygous G2A
332 mice so that tamoxifen injection into the pregnant dam at a specific developmental stage
333 of E10.5, E11.5 and E12.5 (designated as TM10.5, TM11.5 and TM12.5) enabled timed
334 activation of Cre recombinase that initiates reporter (tdTomato) expression in PCs in a
335 birthdate-specific way (Fig. 6A–D). G2A::Ai9 hybrid embryo brain samples were
336 collected between E14.5 and E17.5 (n=23 total: E14.5-TM10.5, n=1; E14.5-TM11.5,
337 n=1; E14.5-TM12.5, n=1; E15.5-TM10.5, n=2; E15.5-TM11.5, n=1; E15.5-TM12.5,
338 n=3; E16.5-TM10.5, n=3; E16.5-TM11.5, n=1; E16.5-TM12.5, n=3; E17.5-TM10.5,
339 n=3; E17.5-TM11.5, n=2; E17.5-TM12.5, n=2), cut into serial sections and
340 immunostained for EphA4, Pcdh10, and either FoxP2 or Corl2. Combined labeling of
341 EphA4 and Pcdh10 helped to recognize the clusters that were identified in the analyses
342 described in the preceding section (Figs. 2–5). No clear difference was observed in the
343 PC cluster organization between G2A::Ai9 mice with C57BL/6 background and wild
344 type mice with B6C3F1 background.

345 Tamoxifen administration labeled neurons with tdTomato in the cerebellum of
346 G2A::Ai9 mice (Fig. 6A–D). The labeling pattern was dependent on the timing of
347 tamoxifen administration but consistent among cases that had the same administration
348 timing. We first checked the specificity and efficiency of the labeling in the E14.5
349 cerebellum. All tdTomato-expressing cells (100%) inside a PC cluster coexpressed a
350 PC-specific marker, Corl2 (Fig. 6F), in all mice (n=23), indicating that tdTomato
351 labeling was specific to PCs. Efficiency of the labeling was estimated by counting the
352 number of tdTomato-expressing PCs among all PCs. Because the majority of PCs are
353 born between E10.5 and E12.5, the sum of the ratios of the tdTomato-labeled PCs in the

354 TM10.5, TM11.5, and TM12.5 cerebellums would become close to 100% if the
355 efficiency is high. Indeed, in the 10,000- μm^2 area of dense PC distribution within the ml
356 cluster of TM10.5, TM11.5, and TM12.5 cerebellums (n=1 each) at E14.5, 41.1% (44
357 PCs out of 107, 44/107), 52.0% (52/100), and 4.7% (5/106) of PCs were
358 tdTomato-positive, respectively, indicating an estimated efficiency of 97.8%. A similar
359 measurement in the c-l cluster showed 1.1% (1/89), 40.8% (40/98) and 45.2% (42/93)
360 labeled PCs in TM10.5, TM11.5 and TM12.5 cerebellums (n=1 each), respectively, at
361 E14.5, indicating an estimated efficiency of 87.1%. The results indicated that the
362 recombination is highly efficient as well as highly dependent on the timing of tamoxifen
363 administration. Similar efficiency and timing-dependency have been also observed in
364 PCs in the adult cerebellum (Zhang et al., 2020). Thus, the PCs labeled by the
365 tamoxifen injection on a specific timing were designated as “E10.5-born” etc. and the
366 area or cluster in which about 1% of PC were labeled with tamoxifen injection at E10.5
367 was designated as “E10.5-PC-sparse”.

368 We then examined the distribution of E10.5-born, E11.5-born and E12.5-born
369 PCs in the PC clusters, which were identified as described in the preceding section, in
370 the E14.5 cerebellum. (Fig. 6A–D and Table 2). E10.5-born PCs were observed densely
371 in the d, ml, and rdl clusters, moderately or sparsely in the c-m, l, dl, and vl clusters (Fig.
372 6A1, B1, C1, D1). However, almost none of the E10.5-born PCs were observed in the m
373 and c-l clusters (blue asterisks in Fig. 6A1, B1, C1). E11.5-born PCs were observed in
374 all clusters (Fig. 6A2, B2, C2, D2). They were more densely distributed in the d, ml,
375 and rdl clusters than in other clusters, and were absent in the medial part of the m cluster.
376 E12.5-born PCs distributed densely in the m cluster and moderately in the c-m, c-l, l,
377 and vl clusters (Fig. 6A3, B3, C3, D3), but rarely contributed to either the d, ml, dl or
378 rdl clusters (orange asterisks in Fig. 6A3, B3, C3, D3). This observation was further
379 quantified by measuring the fluorescence signal intensity, which was supposed to be
380 approximately linearly related to the density of labeled PCs, in each cluster, in digital
381 images of sections of TM10.5, TM11.5 and TM12.5 cerebellums (Fig. 6E). The labeling
382 densities of the c-l and m clusters were near 0, lower than those of other clusters in the
383 TM10.5 cerebellum. but increased to higher levels in the TM11.5 and TM 12.5
384 cerebellums. On the contrary, the labeling densities of the ml, d, and rdl clusters were
385 higher than those of other clusters in the TM10.5 and TM11.5 cerebellums, but
386 decreased to the level near 0, lower than those of other clusters in the TM12.5
387 cerebellum (Fig. 6E).

388 Within each cluster excepting the m cluster, PCs that were born on a particular
389 birthdate appeared to distribute randomly. Boundaries of different labeling density areas

390 matched with the boundaries of the clusters defined by marker expression profiles and
391 PC-free gaps in the TM10.5, TM11.5 and TM12.5 cerebellums (asterisks in Fig. 6A1–3,
392 center subpanels). Each E14.5 cluster was composed of the PCs of two or more
393 particular birthdates (Table 2).

394 In sum, distribution patterns of birthdate-specific PCs were tightly linked with
395 the PC clusters at E14.5. Consequently, the birthdate-specific labeling of PCs were
396 expected to be a useful tool to track the lineage of the 14.5 PC clusters.

397

398 **Tracking birthdate-specific subsets of PCs from E14.5 to E17.5**

399 Since the m and c-l clusters were E10.5-PC-sparse and d, ml, dl and rdl clusters were
400 E12.5-PC-sparse at E14.5 (preceding section), we considered that lineages of these
401 clusters were also E10.5-PC-sparse or E12.5-PC-sparse in later developmental stages.
402 Therefore, we examined distributions of tdTomato-labeled PCs in PC clusters that was
403 identified by immunostaining of Pcdh10 and EphA4 and referring to our preceding
404 analysis of clusters (Fig. 2–5) in serial coronal sections of TM10.5 and TM12.5
405 G2A::Ai9 cerebellums at E14.5, E15.5, E16.5 and E17.5 (Fig. 7). E10.5-PC-sparse
406 clusters and E12.5-PC-sparse clusters were identified among all clustered distinguished
407 at each stage (blue and orange areas in panels of Fig. 7A–D). This observation indicated
408 that medially- and centrolaterally-located E10.5-PC-sparse clusters belonged to the
409 lineage of the m and c-l clusters (designated as m and c-l lineage clusters), respectively,
410 at E15.5–E17.5 (Fig. 7B–D, blue). Similarly, it was indicated that medially-located
411 E12.5-PC-sparse clusters were d lineage clusters, whereas laterally-located
412 E12.5-PC-sparse clusters were either the ml, dl or rdl lineage clusters, respectively (Fig.
413 7B–D, orange). Finally, it was indicated that medially, laterally, and
414 ventrolaterally-located clusters that contained both E10.5-born and E12.5-born PCs
415 were c-m, l, and vl lineage clusters (Fig. 7B–D, neither blue or orange), respectively.

416 The above conclusion was supported by consistency of the marker expression
417 profile of lineage clusters. The m, d, c-m, c-l, l, vl lineage clusters showed similar
418 marker expression profiles to those of their original E14.5 clusters, although minor
419 changes in the expression profile were sometimes recognized in some cases (Table 4).
420 Among ml, dl, and rdl lineage clusters, which were E12.5-born PC-free and located next
421 to one another in the lateral cerebellum, the ml cluster at E14.5 and its daughters, or the
422 ml lineage clusters, at later stages consistently showed strong Pcdh10 expression and
423 were identified consequently (lateral orange in Fig. 7A2, B2, C2, D2). The dl and rdl
424 lineage clusters were distinguished based on denser E10.5-born PCs and Pcdh10
425 expression and more rostralateral positioning of rdl lineage clusters than dl lineage

426 clusters (Table 4). Since their distinction was not necessarily very clear, we sometimes
427 indicate them together by “dl+rdl” in this report.

428 As a whole, the birthdate-specific labeling of PCs allowed us to identify the
429 lineage of all PC clusters between E14.5 and E17.5 (Table 3).

430 At E17.5, the m lineage clusters were located in the most medial area (blue, vt1,
431 vt2, vt3, vc1, vp1-2, in Fig. 7D4), whereas the d lineage clusters were located in the
432 laterally neighboring area (orange, va1, vt5, vt4 in Fig. 7D4). The location of other
433 lineages of clusters was more complicated. All c-m lineage clusters and some c-l lineage
434 clusters were intermingled and located in the intermediate position lateral to the d
435 lineage clusters (grey, vp3-4, ic1-2, ic3 and light blue, ia1-2, va2-4, ip1-2, in Fig. 7D4).
436 More lateral were all ml lineage clusters and some c-l lineage clusters (yellow, it2, ia4
437 and light blue, it3 in Fig. 7D4). All dl+rdl and l lineage clusters and some c-l lineage
438 clusters were located in the most lateral position (yellow, hp2, hc1, ha2, hp4, grey, hc2,
439 ha6, and light blue, ha4 in Fig. 7D4). All vl lineage clusters were located in the
440 ventrolateral edge of the E17.5 cerebellum (not shown in Fig. 7D4).

441 The results demonstrated that the positional relationship among clusters
442 changed in some places during the period between E14.5 and E17.5, indicating that the
443 separate migration of divided clusters is one of the bases for the rearrangement of the
444 compartmental organization of the cerebellum. Furthermore, the marker expression
445 profiles of separated clusters that belonged to the same lineage changed differently to
446 some extent in some cases (Table 4).

447

448 **Spatial differentiation of the c-l lineage clusters during the period from E14.5 to** 449 **E17.5**

450 Among the 37 identified clusters in the E17.5 cerebellum, c-l lineage clusters were
451 located in the most widely-separated areas (light blue, ip1-2, ia1-2, va2-4, it3, ia3-5 and
452 ha4 in Fig. 7D4). Although originating from a single c-l cluster, the c-l lineage clusters
453 were located separately at various rostrocaudal and mediolateral positions in the E17.5
454 cerebellum (Fig. 8G). As described in the preceding section, all the c-l lineage clusters
455 were E10.5-PC-sparse, which facilitated their identification, and showed no expression
456 of Pcdh10 (scarce red or green signals in circumscribed clusters in Fig. 8A–F) and
457 various expression of EphA4 (blue signals in some circumscribed clusters in Fig. 8A–
458 F).

459 To further clarify the spatial differentiation of c-l lineage clusters during the
460 period between E14.5 and E17.5, we examined positional relationships between c-l
461 lineage clusters and neighboring clusters (Fig. 9). At E14.5, the c-l cluster was located

462 lateral to the c-m cluster and medial to the ml cluster: again, the c-l cluster was
463 identified by the weak Pcdh10 expression, weak Corl2 expression and the lack of
464 E10.5-born PCs (Fig. 9A1, Table 2). It occupied the mid-lateral part of the center of the
465 cerebellum with its dorsocaudal part extended laterally to the superficial area dorsal to
466 the ml cluster (Fig. 9A1, B1). The rostral part of the c-l cluster was more extended
467 laterally in the position rostroventral to the ml cluster (arrowheads in Fig. 9A1). The
468 rostromedial part of the c-l cluster had a slightly stronger Corl2 expression than the rest
469 of the c-l cluster (Fig. 9A1, asterisk) and adjoined medially with the c-m cluster which
470 had strong Pcdh10 expression (Fig. 9C1,2).

471 At E15.5, three major rearrangements occurred in the c-l cluster. Firstly, the
472 most medial part of the c-l lineage cluster was recognized as a separate daughter cluster
473 because of its strong Corl2 expression (single asterisk in Fig. 9A2, B2, C2, D2).
474 Secondly, the rostrolateral part of the c-l lineage cluster migrated further laterally in
475 areas rostral and ventral to the ml lineage cluster and increased in EphA4 expression
476 (arrowheads in Fig. 9A2). The caudolateral part of the c-l lineage cluster retracted
477 medially. Lastly, a part of the c-m lineage cluster, which is Pcdh10-positive (Fig. 9A2,
478 B2, double asterisk), migrated laterally at the position ventral to the c-l lineage cluster
479 to separate the ventral portion of the c-l lineage cluster into the rostral and caudal parts
480 (Fig. 9C2, D2).

481 At E16.5, the separation of the c-l cluster that started at E15.5 became clearer.
482 The most lateral part of the c-m lineage cluster further migrated laterally to separate the
483 rostral and caudal parts of the c-l lineage cluster completely (Fig. 9A3, B3, C3, D3,
484 double asterisk). This lateral migration of the c-m lineage cluster confirmed our
485 previous observation with pcdh10 reporter mice (Vibulyaseck et al., 2017). The rostral
486 part of the c-l lineage cluster was spread widely in the mediolateral direction (Fig. 9A3,
487 B3) and subdivided into three daughter subclusters that were recognized by different
488 molecular expression profiles (Fig. 9A3, B3). The lateral daughter subcluster migrated
489 laterally and also elongated caudally (blue in Fig 9B3).

490 At E17.5, the separated c-l lineage clusters (ip1-2, ha4, it3, ia1-2, and va2-4
491 clusters in Fig. 9A4, B4) spread in the mediolateral direction at different rostrocaudal
492 levels. The laterally migrating Pcdh10-positive c-m cluster (ic1-2 cluster) faced the
493 dorsal surface of the cerebellum (Fig. 9C4, D4), as reported previously (Vibulyaseck et
494 al., 2017). The appearance of clear PC-free gaps further firmly separated neighboring
495 daughter clusters (e.g. ia1-2 vs va2-4, in Fig. 9A4). Within these daughter clusters, we
496 noticed a developmental change in EphA4 and Corl2 expression; Corl2 expression
497 became much stronger in the va2-4 cluster than other clusters, while EphA4 expression

498 became stronger in the it3 and ha4 clusters than in the va2-4 and ia1-2 clusters.
499 However, Pcdh10 expression remained weak in these c-l lineage daughter clusters
500 throughout the development from E14.5–17.5 (Fig. 9A4).

501

502 **The lineage of the c-l cluster at adult**

503 Our previous study (Fujita et al., 2012) has suggested that the E17.5 clusters that were
504 identified as the c-l lineage clusters in the present study (va2-4, ia3-5, ia1-2, it3, ha4,
505 and ip1-2 clusters in the E17.5 cerebellum, Fujita et al., 2012) become zebrin-negative
506 and lightly-positive stripes in paravermal and hemispheric areas in the anterior and
507 posterior lobules. We tried to confirm the location of c-l lineage stripes directly in the
508 adult cerebellar cortex by using G2A::Ai9::AldocV mice which show
509 tamoxifen-induced birthdate-dependent labeling of neurons with tdTomato as well as
510 labeling of zebrin-positive PCs with Venus fluorescent protein. We have reported the
511 dependency on tamoxifen injection timing of the general pattern of PC labeling in adult
512 G2A::Ai9::AldocV mice (Zhang et al., 2020). Here, we mapped E10.5-PC-sparse
513 cortical areas (Fig. 10A) by the observation of cerebellar sections of G2A::Ai9::AldocV
514 mice that received tamoxifen at E10.5 (n=2 mice) to identify c-l lineage stripes.

515 In the adult mouse cerebellar cortex, the striped expression pattern of zebrin
516 (aldolase C) is consistent across individuals and has been identified in detail (Fujita et
517 al., 2014; Sarpong et al., 2018). Accordingly, zebrin stripes are described here by using
518 the common nomenclature (Fujita et al., 2014; Sarpong et al., 2018). Zebrin stripes are
519 mostly designated with a numeral or an alphabet character followed by “+” or “-” (Fig.
520 1C). Note that a pair of stripes in the anterior and posterior lobules, which are named
521 differently, together belongs to the same cerebellar module, because they receive
522 common branching olivocerebellar axons (Sugihara and Shinoda, 2004): for example, a
523 pair of 4+ stripe in anterior lobules and 5+ stripe in posterior lobules form the C2
524 module and thus considered to be the same or linked stripe, which is designated as
525 “4+//5+”.

526 In lobules I-V, except for stripe 2+ and the medial part of stripe 2-, most of the
527 paravermal stripes (the lateral part of zebrin stripes 2-, stripes b+, b-, 3+ and 3-) were
528 E10.5-PC-sparse and consequently identified as the fate of c-l lineage clusters (the right
529 circumscribed areas in Fig. 10B1). However, the most lateral part of stripe 3- and the
530 entire stripe 4+ contained a high density of E10.5-born PCs. Most of stripe 4- was
531 E10.5-PC-sparse (the left circumscribed area in Fig. 10B1). The most lateral part of
532 stripe 4- and entire stripe 5+ contained a high density of E10.5-born PCs. Stripe 5- was
533 E10.5-PC-sparse (the left ventral circumscribed area in Fig. 10B1).

534 In the simple lobule, most of the medial paravermal area had a low-dense
535 distribution of E10.5-born PCs (double asterisks in Fig. 10B1). This area was likely to
536 be derived from c-m lineage clusters, which had similarly a low density of E10.5-born
537 PCs in the embryonic cerebellum (Fig. 7D). This agrees to the speculation of our
538 previous study that this area originates from E17.5 clusters ic1 and ic2 (Fujita et al.,
539 2012), which originated from the E14.5 c-m cluster in the present result (Table 2).
540 Zebrin positive stripe 4+ and medially adjacent zebrin negative area contained a high
541 density of E10.5-born PCs. On the contrary, stripe 4-, except for its lateral part, was
542 E10.5-PC-sparse. Stripe 4- was also E10.5-PC-sparse in crus I (the most left
543 circumscribed area in Fig. 10B1). These E10.5-PC-sparse areas were identified as the
544 fate of c-l lineage clusters (circumscribed in Fig. 10B1) occupied a relatively large
545 portion in the paravermal cerebellar cortex in the rostral cerebellum.

546 Some tdTomato labeling in the molecular layer inside the circumscribed areas
547 indicated the presence of labeled PC dendrite (left magenta labeling in the inset in Fig.
548 10B1). However, the number of labeled somata that were located within the section
549 (arrowheads in Fig. 10B1-4) was rather small (12 PCs in Panel B1, roughly 1-2%
550 against the denominator of all PC somata, ~700, recognized in the background inside
551 the circumscribed areas), supporting our description “mostly lacking” and
552 “E10.5-PC-sparse”. This percentage (1-2%) was approximately the same as the number
553 of labeled PCs inside the E14.5 c-l cluster (preceding section).

554 In the rest of cerebellar lobules (lobules VI-X, crus I, crus II, paramedian
555 lobule, copula pyramidis, paraflocculus and flocculus), several areas were
556 E10.5-PC-sparse and identified as the fate of the c-l clusters. These areas included the
557 lateral part of stripe 2- in lobules V-VI (circumscribed in Fig. 10B2), the medial part of
558 stripe 5- in crus II (circumscribed in Fig. 10B2-B3), and multiple zebrin-negative and
559 faintly zebrin positive stripes in the copula pyramidis and adjacent paramedian lobule
560 (circumscribed in Fig. 10B2, B4). Distribution of E10.5-born PCs in the medial
561 paravermal areas in crus I, crus II and paramedian lobule, which are likely to belong to
562 c-m lineage areas (Fujita et al., 2012, Vibryaseck, 2017), appeared a little denser
563 (double asterisks in Fig. 10 B2-4) than the c-l lineage areas. Other stripes in the
564 paravermal and hemispheric areas had a rather dense distribution of E10.5-born PCs.

565 The E10.5-PC-sparse zebrin stripes that were considered to belong to the c-l
566 lineage were mapped on the unfolded scheme of the entire cerebellar cortex with the
567 zebrin (aldolase C) striped pattern (Fig. 10F; Fujita et al., 2014; Sarpong et al., 2018).
568 The c-l lineage areas were located in zebrin-negative and weakly-positive stripes in the
569 lateral vermis and paravermis in lobules I-V and VIII/copula pyramidis (red and green

570 in Fig. 10F), and in the medial hemisphere in lobules I-V, simple lobule, crus II and
571 paramedian lobule (blue in Fig. 10F). However, no c-l lineage areas were observed in
572 the central part (lobules VI-VII and apex of crus I) of the cerebellum. Based on the
573 correspondence between the zebrin stripes and cerebellar modules (Sugihara et al., 2004,
574 2009), the mapped stripes corresponded to the B module (red in Fig. 10F), which
575 projects to the lateral vestibular nucleus (Sugihara et al., 2009; Ruigrok et al., 2015),
576 and most of the C1, C3 and D0 modules, which project to the anterior interposed
577 nucleus (green and blue in Fig. 10F, Table 5). The results demonstrated that the
578 separation and migration of the c-l cluster during development forms multiple stripes
579 that mainly correspond to the anterior and posterior parts of the C1/C3 module (Fig.
580 10C-F), and also the B module and a part of the D0 module.

581

582 **Discussion**

583 The present study demonstrated the spatial development of the compartmental
584 organization of the mouse embryonic cerebellum between E14.5 and E17.5. The
585 lineages of the nine E14.5 PC clusters which transformed into 37 clusters at E17.5 were
586 tracked by birthdate-tagging. Furthermore, it was shown that one of the E14.5 clusters
587 named c-l differentiated into several zebrin stripes that belong to the C1/C3 module in
588 the anterior and posterior lobules. The results supported our hypothesis that the
589 rearrangement of embryonic PC clusters shapes the compartmentalization of the adult
590 cerebellar cortex which may underlie its modular organization and the dual somatotopy.

591

592 **Cerebellar compartmental organization originate from the differentiation of early** 593 **PC clusters**

594 The present study revealed a progressive change in the compartmental organization in
595 the embryonic cerebellum. The number of PC clusters recognized by the marker
596 molecule expression profile increased from nine at E14.5 to 37 at E17.5. This increase
597 was accompanied by a significant change in the spatial arrangement of PC clusters
598 between E14.5 and E17.5, as demonstrated in the separation and migration of the c-l
599 lineage clusters in the present study. Since the clustered compartments of PCs in the late
600 embryonic stage (E17.5 in mice) are mostly comparable to the striped compartments of
601 PCs in the adult (Fujita et al., 2012), our clarification of the compartmental
602 differentiation in the period before E17.5 would lead to a better understanding (see
603 below, "Developmental origin of the dual representation of the somatosensorimotor
604 function in the cerebellum") of adult cerebellar compartmentalization. Compartmental
605 organization at stages earlier than E14.5 was beyond the scope of the present study.

606 Concerning marker molecules used in this study, we speculate that transcription
607 factors FoxP2 and Corl2 may control the expression of compartment-specific molecules,
608 and adhesion molecule Pcdh10 and receptor tyrosine kinase EphA4 may be involved in
609 cluster formation and cell-to-cell connection between highly-expressing neurons
610 (Vibulyaseck et al., 2017; Sarpong et al, 2018), the functional significance of these
611 marker molecules in the development of PC compartmentalization has not been fully
612 clarified. Nevertheless, differences in their expression levels among PCs were useful to
613 detect trackable PC clusters in the present study. Based on different expression
614 intensities of these marker molecules, we distinguished PC clusters in the entire
615 cerebellum in embryonic dates between E14.5 and E17.5 (Fig. 2-5, Table 2)

616 The PC cluster organization identified in our study conformed to the PC
617 organization that was identified based on gene expression profiling analysis at E14.5
618 (Wizeman et al., 2019), except for the *Nrgn*-positive cluster. The *Nrgn*-positive cluster,
619 which is located widely above the ventricular zone and under other clusters (Wizeman
620 et al., 2019), was not recognized as a cluster in our present study. *Nrgn* mRNA is
621 expressed in neuro-progenitor and immature neurons in cerebral cortical culture (Nazir
622 et al., 2018). Therefore, there is a possibility that *Nrgn*-positive cluster of Wizeman et al.
623 (2019) represents newly-born PCs that are joining one of the other clusters. Besides, six
624 of our nine E14.5 PC clusters m, c-m, c-l, d, ml, and l corresponded to clusters Ebf,
625 Ebf/Calb1, *Nrgn*/Calb1, Ebf/Dab1-dorsal, Ebf/Dab1-ventral and Foxp1/Dab1 in Fig. 4H
626 of Wizeman et al. (2019), respectively. It would mean that our PC clusters defined by
627 marker molecule expression and PC birthdate and PC clusters defined by gene
628 expression profiling make one-to-one correspondence, except for the *Nrgn*-positive
629 cluster (above), at the caudal level of the cerebellum. The correspondence of three of
630 our nine E14.5 clusters (dl, rd1 and vl) was not known because they were located at the
631 more rostral level than the section shown in Wizeman et al. (2019). As a whole, the high
632 consistency between our E14.5 cluster recognition and PC gene expression profiling
633 support the cluster assembly that we recognized here represents not an arbitrarily
634 defined structure but an essential organization of the E14.5 cerebellum.

635

636 **Birthdate-specific neuronal labeling to track the lineage of early PC compartments**

637 Tracing the lineage of early PC clusters in the embryonic cerebellum by
638 birthdate-specific labeling of PCs was the essential method in this study. Since PCs of
639 different birthdates are distributed heterogeneously in different PC compartments
640 (Hashimoto et al., 2003; Namba et al., 2011), birthdate-specific labeling of PCs can be a
641 useful experimental tool to track the lineage of PC clusters. Indeed, the original

642 birthday-specific labeling with the *ascl1* gene CreER-LoxP system showed that PCs
643 labeled by tamoxifen given at E10.5, E11.5 and E12.5 are distributed differently in the
644 adult cerebellum (Sudarov et al., 2011). Such a birthdate-specific labeling system is
645 technically more accessible and appears more sensitive than previously established
646 birthdate-specific labeling methods (systemic injection of 5-bromo-2'-deoxyuridine,
647 BrdU; systemic injection of tritium-labeled thymidine, Altman et al., 1985; or in-utero
648 ventricular injection of replication-defective adenoviral vector, Hashimoto et al., 2004;
649 Namba et al., 2011). G2A mice, in which the *Neurog2* gene is targeted, allowed us to
650 efficiently produce specimens with varying tamoxifen injection dates and survival
651 periods in the present study. The labeling pattern of birthdate-specific PCs in the adult
652 cerebellum in the present study was similar but not the same as that reported with
653 adenoviral vector labeling (Namba et al., 2011). For example, E11.5-born PCs were
654 observed in most of the embryonic PC clusters and the majority of adult zebrin stripes
655 in G2A mice (the present study and Zhang et al., 2020), they were distributed in a
656 smaller number of PC compartments in adenoviral vector labeling. Such discrepancies
657 may be due to some differences in the timing (e.g. different cell cycle points, different
658 durations/efficiencies of labeling activity, etc.) of labeling differentiating neurons
659 between different methods.

660

661 **Developmental origin of the dual representation of the somatosensorimotor** 662 **function in the cerebellum**

663 The birthdate-tagging method employed in the present study revealed that the
664 anteroposteriorly- and mediolaterally-separated stripes belonging to the
665 somatosensorimotor C1/C3 modules originate mostly from the c-l cluster at E14.5,
666 which is composed of E11.5- and E12.5 born PCs (Fig. 10C-F). The mediolateral
667 separation of the c-l cluster, the anteroposterior separation of the C1 module occurred in
668 the medial c-l lineage cluster at E15.5. Besides, the anteroposterior separation of the C3
669 module occurs in the early postnatal period in the cluster which originates from the
670 lateral c-l lineage cluster at E14.5 by the lateral migration of the ml lineage cluster (Fig.
671 10E, it3 cluster to be separated anteroposteriorly by ic5/it2 cluster) as shown previously
672 (Fujita et al., 2012). Although the timing is different, the anatomical process of
673 anteroposterior separation seems similar between these two modules. To further
674 understand this differentiation process, causal mechanisms that induce rostrocaudal
675 separation of c-l lineage clusters are to be studied. The rostro-caudal link has been
676 generally observed in axonal projections in compartments in paravermal and
677 hemispheric modules (Sugihara and Shinoda, 2004; Fujita and Sugihara, 2013). We

678 could not observe evidence of the anteroposterior separation of the B module or the
679 most medial Corl2-strongly positive c-l lineage cluster, as well as evidence of the
680 anteroposterior separation of the D0 module or the most lateral c-l lineage cluster during
681 the embryonic period in the present study, either.

682 Purkinje cells themselves play an essential role in the formation of the
683 topographic afferent and efferent circuits (Sillitoe et al., 2009, 2010; White et al., 2014).
684 The PC axonal projection and the olivocerebellar projection are directly linked to the
685 compartmental or modular organization of the cerebellar cortex (Sugihara et al., 2004;
686 Sugihara et al., 2009; Cerminara et al., 2013, Fig. 10F, Table 5). Single climbing fiber
687 axons typically branch rostrocaudally and innervate both the anterior and posterior parts
688 of the same module (Sugihara et al., 2001; Fujita and Sugihara, 2013). Axonal
689 projections of PCs in the anterior and posterior parts of the same module converge on
690 the same small area in the cerebellar nucleus (Sugihara et al., 2009). Such a rostrocaudal
691 relationship in axonal projections is understandable by supposing the same axonal
692 guidance cues (Sillitoe et al., 2009, 2010) expressed by the pair of rostral and caudal PC
693 clusters that originated from the same early cluster. Since PC compartments are
694 topographically connected with subareas of the cerebellar nuclei and inferior olive
695 (Ruigrok et al., 2015), the development of the cerebellar modules may depend on the
696 mutual development of the compartments in the cerebellar cortex, cerebellar nuclei, and
697 inferior olive. Indeed, a genetically-induced defect in the developing cerebellar nuclei
698 produces malformation of the cerebellar cortex (Willett et al., 2019). However, the
699 development of compartments of the cerebellar nuclei or inferior olive has not been
700 clarified yet to the level comparable to the fine compartmentalization shown in the
701 cerebellar cortex (Fujita et al., 2012; Fujita et al., 2020).

702 The mossy fiber projection, which is the main source of afferent axons to the
703 cerebellar cortex, is not as tightly linked to PC compartments as PC axons or
704 olivocerebellar axons (Quy et al., 2011; Biswas et al., 2019; Luo et al. 2020). However,
705 because early mossy fibers initially target PCs (Kalinovsky et al., 2011), the early PC
706 cluster organization may affect the mossy fiber projection pattern. Indeed, single mossy
707 fibers often show branching to the anterior and posterior cerebellums (Biswas et al.,
708 2019), which is similar to the anteroposterior separation of PC clusters shown in the
709 present study. As a whole, the present study showed that the spatiotemporal
710 differentiation process of early PC compartmentalization underlies the anteroposterior
711 dual positioning of somatotopic areas in the cerebellar cortex (Snider et al., 1950;
712 Stoodley et al., 2012; Guell et al., 2018), one of the most peculiar characteristics of
713 cerebellar functional localization.

714 The present results propose a hypothesis about the general origin of the
715 cerebellar compartmentalization: adult cerebellar compartments that share similar
716 molecular expression profiles, axonal projections, and functional localization may
717 generally originate from a common early PC compartment in cerebellar development.
718 Besides the C1/C3 modules, our previous finding that the ml cluster at E14.5 became
719 zebrin stripe 4+//5+ (4+ in the anterior cerebellum and 5+ in the posterior cerebellum),
720 or the C2 module (Vibulyaseck et al., 2017) supports this hypothesis. However, the
721 experimental results were not as simple. For example, the most medial part of the c-l
722 cluster showed an increase in expression of *Corl2* and was distinguished from the rest of
723 the c-l cluster at E15.5 (Fig. 9A). It became stripes 2- and b+, forming the B module,
724 which projects to the lateral vestibular nucleus (Sugihara et al., 2009) for the control of
725 posture and anti-gravity through the lateral vestibulospinal projection (Voogd, 2016),
726 and quite distinct from the C1/C3 modules. B module does not only occupy a
727 substantial area in the anterior cerebellum but also present in the posterior cerebellum,
728 in a small lateral vermal area of lobule VIII (stripe 4-, Fig. 10B4; Sugihara et al., 2009).
729 The origin of this caudal B module was not clarified in the present study. The
730 centrolateral part of the c-l cluster formed zebrin stripes 4-//5- (4- in the anterior
731 cerebellum and 5- in the posterior cerebellum, Fig. 10F) or the C3 module. The
732 separation of stripe 4-//5- into medial and lateral substripes has been reported in our
733 analysis of the PC birthdates in the adult cerebellar cortex (Zhang et al., 2020). It was
734 noticeable that only the medial substripe of 4-//5- originated from the c-l cluster.
735 Consequently, the lateral substripe of 4-//5- is supposed to originate from a different
736 cluster at E14.5. The most lateral part of the c-l cluster formed a small part of
737 zebrin-negative stripe 5-//6- or the D0 module (Sugihara et al., 2004). The D0 module is
738 the somatosensorimotor module akin to the C1/C3 modules and containing the area
739 involved in the eye-blinking reflex (Attwell et al., 2001). According to the present
740 results, most parts of the D0 module including the entire caudal parts of the D0 module
741 in the posterior cerebellum, seem to originate from different clusters. Thus, several
742 interesting questions remain unclear regarding functional domains delineated by
743 embryonic clusters and adult striped organization. The relationship between the early
744 PC compartmentalization and the mossy fiber projection pattern is also to be studied.

745

746

747 **References**

- 748 Altman J, Bayer SA (1985) Embryonic development of the rat cerebellum. I.
749 delineation of the cerebellar primordium and early cell movements. *J Comp Neurol*
750 231:1-26.
- 751 Apps R, Hawkes R (2009) Cerebellar cortical organization: A one-map hypothesis.
752 *Nature Reviews Neuroscience* 10:670-681.
- 753 Attwell PJ, Rahman S, Yeo CH (2001) Acquisition of eyeblink conditioning is
754 critically dependent on normal function in cerebellar cortical lobule HVI. *Journal of*
755 *Neuroscience* 21:5715-5722.
- 756 Biswas MS, Luo Y, Sarpong GA, Sugihara I (2019) Divergent projections of single
757 pontocerebellar axons to multiple cerebellar lobules in the mouse. *J Comp Neurol*
758 527:1966-1985.
- 759 Brochu G, Maler L, Hawkes R (1990) Zebrin II: A polypeptide antigen expressed
760 selectively by Purkinje cells reveals compartments in rat and fish cerebellum. *J Comp*
761 *Neurol (United States)* 291:538-552.
- 762 Carter RA, Bihannic L, Rosencrance C, Hadley JL, Tong Y, Phoenix TN, Natarajan S,
763 Easton J, Northcott PA, Gawad C (2018) A single-cell transcriptional atlas of the
764 developing murine cerebellum. *Current Biology* 28:2910-2920. e2.
- 765 Cerminara NL, Aoki H, Loft M, Sugihara I, Apps R (2013) Structural basis of
766 cerebellar microcircuits in the rat. *Journal of Neuroscience* 33:16427-16442.
- 767 Ekerot C, Garwicz M, Jörntell H (1997) The control of forelimb movements by
768 intermediate cerebellum. In: *Progress in brain research The control of forelimb*
769 *movements by intermediate cerebellum.* pp423-429.Elsevier.
- 770 Florio M, Leto K, Muzio L, Tinterri A, Badaloni A, Croci L, Zordan P, Barili V,
771 Albieri I, Guillemot F (2012) Neurogenin 2 regulates progenitor cell-cycle
772 progression and Purkinje cell dendritogenesis in cerebellar development.
773 *Development* 139:2308-2320.
- 774 Fujita H, Aoki H, Ajioka I, Yamazaki M, Abe M, Oh-Nishi A, Sakimura K, Sugihara
775 I (2014) Detailed expression pattern of aldolase C (aldoc) in the cerebellum, retina
776 and other areas of the CNS studied in aldoc-venus knock-in mice. *PLoS One (United*
777 *States)* 9:e86679.
- 778 Fujita H, Sugihara I (2013) Branching patterns of olivocerebellar axons in relation to
779 the compartmental organization of the cerebellum. *Frontiers in Neural Circuits* 7:3.
- 780 Fujita H, Morita N, Furuichi T, Sugihara I (2012) Clustered fine
781 compartmentalization of the mouse embryonic cerebellar cortex and its
782 rearrangement into the postnatal striped configuration. *Journal of Neuroscience*
783 32:15688-15703.

- 784 Fujita H, Kodama T, du Lac S. (2020) Modular output circuits of the fastigial nucleus
785 for diverse motor and nonmotor functions of the cerebellar vermis. *eLife* 9:e58613.
- 786 Goffinet AM (1983) The embryonic development of the cerebellum in normal and
787 reeler mutant mice. *Anat Embryol* 168:73-86.
- 788 Guell X, Schmahmann JD, Gabrieli JD, Ghosh SS (2018) Functional gradients of the
789 cerebellum. *Elife* 7:e36652.
- 790 Hashimoto M, Mikoshiba K (2004) Neuronal birthdate-specific gene transfer with
791 adenoviral vectors. *Journal of Neuroscience* 24:286-296.
- 792 Hashimoto M, Mikoshiba K (2003) Mediolateral compartmentalization of the
793 cerebellum is determined on the “birth date” of Purkinje cells. *Journal of*
794 *Neuroscience* 23:11342-11351.
- 795 Hirata T, Shioi G, Abe T, Kiyonari H, Kato S, Kobayashi K, Mori K, Kawasaki T
796 (2019) A novel birthdate-labeling method reveals segregated parallel projections of
797 mitral and external tufted cells in the main olfactory system. *eNeuro* 6:6.
- 798 Horn KM, Pong M, Gibson AR (2010) Functional relations of cerebellar modules of
799 the cat. *Journal of Neuroscience* 30:9411-9423.
- 800 Kalinovsky A, Boukhtouche F, Blazeski R, Bornmann C, Suzuki N, Mason CA,
801 Scheiffele P (2011) Development of axon-target specificity of ponto-cerebellar
802 afferents. *PLoS Biology* 9:2.
- 803 Korneliussen HK (1968) On the ontogenetic development of the cerebellum (nuclei,
804 fissures, and cortex) of the rat, with special reference to regional variations in
805 corticogenesis. *J Hirnforsch* 10:379.
- 806 Larouche M, Che PM, Hawkes R (2006) Neurogranin expression identifies a novel
807 array of Purkinje cell parasagittal stripes during mouse cerebellar development. *J*
808 *Comp Neurol* 494:215-227.
- 809 Low AY, Thanawalla AR, Yip AK, Kim J, Wong KL, Tantra M, Augustine GJ, Chen
810 AI (2018) Precision of discrete and rhythmic forelimb movements requires a distinct
811 neuronal subpopulation in the interposed anterior nucleus. *Cell Reports*
812 22:2322-2333.
- 813 Luo Y, Onozato T, Wu X, Sasamura K, Sakimura K, Sugihara I (2020) Dense
814 projection of Stilling's nucleus spinocerebellar axons that convey tail proprioception
815 to the midline area in lobule VIII of the mouse cerebellum. *Brain Struct Funct*
816 225:621-638.
- 817 Luo Y, Patel RP, Sarpong GA, Sasamura K, Sugihara I (2018) Single axonal
818 morphology and termination to cerebellar aldolase C stripes characterize distinct

819 spinocerebellar projection systems originating from the thoracic spinal cord in the
820 mouse. *J Comp Neurol* 526:681-706.

821 Manni E, Petrosini L (2004) A century of cerebellar somatotopy: a debated
822 representation. *Nat Rev Neurosci* 5:241-249.

823 Millen KJ, Hui C, Joyner AL (1995) A role for en-2 and other murine homologues of
824 drosophila segment polarity genes in regulating positional information in the
825 developing cerebellum. *Development* 121:3935-3945.

826 Minaki Y, Nakatani T, Mizuhara E, Inoue T, Ono Y (2008) Identification of a novel
827 transcriptional corepressor, *Corl2*, as a cerebellar Purkinje cell-selective marker.
828 *Gene Expression Patterns* 8:418-423.

829 Namba K, Sugihara I, Hashimoto M (2011) Close correlation between the birth date
830 of Purkinje cells and the longitudinal compartmentalization of the mouse adult
831 cerebellum. *J Comp Neurol* 519:2594-2614.

832 Nazir FH, Becker B, Brinkmalm A, Höglund K, Sandelius Å, Bergström P, Satir TM,
833 Öhrfelt A, Blennow K, Agholme L (2018) Expression and secretion of synaptic
834 proteins during stem cell differentiation to cortical neurons. *Neurochem Int*
835 121:38-49.

836 Oberdick J, Schilling K, Smeyne RJ, Corbin JG, Bocchiaro C, Morgan JI (1993)
837 Control of segment-like patterns of gene expression in the mouse cerebellum. *Neuron*
838 10:1007-1018.

839 Pijpers A, Winkelman BH, Bronsing R, Ruigrok TJ (2008) Selective impairment of
840 the cerebellar C1 module involved in rat hind limb control reduces step-dependent
841 modulation of cutaneous reflexes. *Journal of Neuroscience* 28:2179-2189.

842 Quy PN, Fujita H, Sakamoto Y, Na J, Sugihara I (2011) Projection patterns of single
843 mossy fiber axons originating from the dorsal column nuclei mapped on the aldolase
844 C compartments in the rat cerebellar cortex. *J Comp Neurol* 519:874-899.

845 Ruigrok TJ, Sillitoe RV, Voogd J (2015) Cerebellum and cerebellar connections. In:
846 Paxinos G. ed, *The Rat Nervous System*. 4th ed. pp133-205. Amsterdam, Elsevier
847 Academic Press.

848 Sarpong GA, Vibulyaseck S, Luo Y, Biswas MS, Fujita H, Hirano S, Sugihara I
849 (2018) Cerebellar modules in the olivo-cortico-nuclear loop demarcated by *pcdh10*
850 expression in the adult mouse. *J Comp Neurol* 526:2406-2427.

851 Sillitoe RV, Joyner AL (2007) Morphology, molecular codes, and circuitry produce
852 the three-dimensional complexity of the cerebellum. *Annu Rev Cell Dev Biol*
853 23:549-577.

- 854 Sillitoe RV, Vogel MW, Joyner AL (2010) Engrailed homeobox genes regulate
855 establishment of the cerebellar afferent circuit map. *Journal of Neuroscience*
856 30:10015-10024.
- 857 Sillitoe RV, Gopal N, Joyner AL (2009) Embryonic origins of ZebrinII parasagittal
858 stripes and establishment of topographic Purkinje cell projections. *Neuroscience*
859 162:574-588.
- 860 Smeyne RJ, Oberdick J, Schilling K, Berrebi AS, Mugnaini E, Morgan JI (1991)
861 Dynamic organization of developing Purkinje cells revealed by transgene expression.
862 *Science* 254:719-721.
- 863 Snider RS (1950) Recent contributions to the anatomy and physiology of the
864 cerebellum. *Archives of Neurology & Psychiatry* 64:196-219.
- 865 Stoodley CJ, Valera EM, Schmahmann JD (2012) Functional topography of the
866 cerebellum for motor and cognitive tasks: An fMRI study. *Neuroimage*
867 59:1560-1570.
- 868 Sudarov A, Turnbull RK, Kim EJ, Lebel-Potter M, Guillemot F, Joyner AL (2011)
869 *Ascl1* genetics reveals insights into cerebellum local circuit assembly. *Journal of*
870 *Neuroscience* 31:11055-11069.
- 871 Sugihara I, Shinoda Y (2004) Molecular, topographic, and functional organization of
872 the cerebellar cortex: A study with combined aldolase C and olivocerebellar labeling.
873 *Journal of Neuroscience* 24:8771-8785.
- 874 Sugihara I, Wu HS, Shinoda Y (2001) The entire trajectories of single olivocerebellar
875 axons in the cerebellar cortex and their contribution to cerebellar
876 compartmentalization. *J Neurosci* 21:7715-7723.
- 877 Sugihara I, Fujita H, Na J, Quy PN, Li B, Ikeda D (2009) Projection of reconstructed
878 single Purkinje cell axons in relation to the cortical and nuclear aldolase C
879 compartments of the rat cerebellum. *J Comp Neurol* 512:282-304.
- 880 Thickbroom GW, Byrnes ML, Mastaglia FL (2003) Dual representation of the hand
881 in the cerebellum: activation with voluntary and passive finger movement.
882 *NeuroImage* 18:670-674.
- 883 Vibulyaseck S, Fujita H, Luo Y, Tran AK, Oh-Nishi A, Ono Y, Hirano S, Sugihara I
884 (2017) Spatial rearrangement of Purkinje cell subsets forms the transverse and
885 longitudinal compartmentalization in the mouse embryonic cerebellum. *J Comp*
886 *Neurol* 525:2971-2990.
- 887 Voogd J, Glickstein M (1998) The anatomy of the cerebellum. *Trends Neurosci*
888 (England) 21:370-375.

- 889 Voogd J (2016) Deiters' nucleus. its role in cerebellar ideogenesis. *The Cerebellum*
890 15:54-66.
- 891 Welker W (1987) Spatial Organization of Somatosensory Projections to Granule Cell
892 Cerebellar Cortex: Functional and Connectional Implications of Fractured
893 Somatotopy (Summary of Wisconsin Studies). In: *New Concepts in Cerebellar*
894 *Neurobiology*, pp239-280. New York, Alan R Liss.
- 895 White JJ, Arancillo M, Stay TL, George-Jones NA, Levy SL, Heck DH, Sillitoe RV.
896 (2014) Cerebellar zonal patterning relies on Purkinje cell neurotransmission. *J*
897 *Neurosci* 34(24):8231-8245.
- 898 Willett RT, Bayin NS, Lee AS, Krishnamurthy A, Wojcinski A, Lao Z, Stephen D,
899 Rosello-Diez A, Dauber-Decker KL, Orvis GD, Wu Z, Tessier-Lavigne M, Joyner
900 AL (2019) Cerebellar nuclei excitatory neurons regulate developmental scaling of
901 presynaptic Purkinje cell number and organ growth. *Elife* 8:e50617.
- 902 Wilson SL, Kalinovsky A, Orvis GD, Joyner AL (2011) Spatially restricted and
903 developmentally dynamic expression of engrailed genes in multiple cerebellar cell
904 types. *The Cerebellum* 10:356-372.
- 905 Wizeman JW, Guo Q, Wilion EM, Li JY (2019) Specification of diverse cell types
906 during early neurogenesis of the mouse cerebellum. *eLife* 8:e42388.
- 907 Zhang J, Tran-Anh K, Hirata T, Sugihara I (2020) Striped distribution pattern of
908 Purkinje cells of different birthdates in the mouse cerebellar cortex studied with the
909 *Neurog2-CreER* transgenic line. *Neuroscience* doi:
910 10.1016/j.neuroscience.2020.07.028. Online ahead of print.
- 911 Zordan P, Croci L, Hawkes R, Consalez GG (2008) Comparative analysis of
912 proneural gene expression in the embryonic cerebellum. *Developmental Dynamics:*
913 *An Official Publication of the American Association of Anatomists* 237:1726-1735.
914

915 Table 1: Antibodies used in the study

916

	Antigen	Manufacturer, species, mono- or polyclonal, catalog or lot No., RRID	Concentration
Primary Antibodies	Corl2	Dr. Yuichi Ono (KAN Research Institute), rabbit polyclonal, affinity-purified	1:350
	EphA4	R&D Systems, goat polyclonal, Cat# AF641, Lot #BVX0308091	1:1000
	FoxP2	Everest Biotech (Oxfordshire, UK), goat polyclonal, Cat# EB05226, Lot # 160409, RRID: AB_2107112	1:5000
	FoxP2	Abgent, rabbit polyclonal, Cat# AP5753b, Lot #SA100916AA, RRID: AB_10818782	1:1000
	Pcdh10	Millipore, rat monoclonal, clone 5G10, Cat# MABT20, Lot # NRG1759424, RRID:AB_10807416	1:1600
	Calbindin D28	Sigma, mouse monoclonal, Cat# 175651C8666	1:500
Secondary Antibodies	Anti-Goat IgG, Alexa Fluor 488	Jackson ImmunoResearch, donkey, Cat# 705-545-147	1:400
	Anti-Goat IgG, Alexa Fluor 680	Jackson ImmunoResearch, donkey, Cat# 705-625-147	1:400
	Anti-Rabbit IgG, Alexa Fluor 405	abcam, donkey, Cat# 175651	1:500
	Anti-Rabbit IgG, Alexa Fluor 488	Jackson ImmunoResearch, donkey, Cat# 711-545-152	1:400

	Anti-Rabbit IgG, Alexa Fluor 647	Jackson ImmunoResearch, donkey, Cat# 711-605-152	1:400
	Anti-Rabbit IgG, Alexa Fluor 594	Jackson ImmunoResearch, donkey, Cat# 711-585-152	1:400
	Anti-Rabbit IgG, Teas Red	Jackson ImmunoResearch, donkey, Cat# 711-075-152	1:200
	Anti-Rat IgG, DyLight 594	Jackson ImmunoResearch, donkey, Cat# 712-515-153	1:200
	Anti-Rat IgG, Alexa Fluor 647	Jackson ImmunoResearch, donkey, Cat# 705-605-150	1:400
	Anti-Rat IgG, Alexa Fluor 680	abcam. donkey, Cat# 175777	1:500
	Anti-Mouse IgG, Alexa Fluor 647	Jackson ImmunoResearch, donkey, Cat# 715-605-150	1:400

917

918 Table 2: Nine E14.5 PC clusters, their molecular expression profiles, PC birthdates and
 919 fates at E17.5
 920

E14.5 PC cluster		m	d	c-m	c-l	ml	dl	rdl	l	vl
Molecular expression profile	Corl2	+ ~ +++	++	+++	++	+	+++	+++	++	++
	Pcdh10	- ~ ++	++	+ ~ +++	+/-	+++	+/-	++	+	+/-
	EphA4	- ~ ++	-	++	++	+++	++	+++	++	+/-
	FoxP2	+ ~ +++	+++	+	++	+++	++	+++	++	-
PC birthdate		- E11.5, E12.5	E10.5, E11.5, -	E10.5, E11.5, E12.5	- E11.5, E12.5	E10.5, E11.5, -	E10.5, E11.5, -	E10.5, E11.5, -	E10.5, E11.5, E12.5	E10.5, E11.5, E12.5
fate at E17.5 (E17.5 cluster)		vt1, vt2, vc1, vp1-2, vt3, no1-2	vt4, vt5, va1	vp3-4, ic1-2, no4, no5, no3, ic3	va2-4, ip1-2, ia1-2, it3, ha4, ia3-5	it2, ia4	hp1-2, hc1, ha1, ha2-3	hp3, hp4, pf	ha5, ha6, hc2	fl1-2, fl3, fl4, fl5

921

922

923 Table 3: Definition of E17.5 PC clusters

924

Cluster	Definition in Fujita et al. 2012	caudorostral levels	Corl2	Pcdh10	EphA4	FoxP2	Calbindin
vt1	vt1	6-58%	+	++	-	+	++
vt2	vt2	10-58%	+++	+	++	++	-
vc1	vc1	6-27%	+++	+++	++	+++	+
vt3	vt3	6-58%	++	+++	+	+++	+
vp1-2	vp1, vp2	6-18%	++	+	++	+++	+
vt4	vt4	6-58%	+	++	++	+	+
vt5	vt5	10-52%	++	+	-	+	-
va1	va1	13-36%	++	++	++	+++	+
va2-4	va2, va3, va4	6-52%	+++	+	-	++	+
ia1-2	ia1, ia2	42-55%	+	+	-	++	-
ip1-2	ip1, ip2	10-23%	+	+	-	++	-
vp3-4	vp3, vp4, vc2	6-19%	+++	+	+++	+++	+
ic1-2	ic1, ic2	10-26%	+++	+++	+++	++	+
it2	it2, ic5, ip3	23-55%	++	+++	-	++	+
ic3	ic3	23-39%	+	+	+++	+++	-
ia4	ia4, ic4	26-49%	++	+	-	++	-
it3	it3	25-80%	++	+	+++	++	-
ia3-5	ia3, ia5	62-71%	++	+	+++	+++	-
ha4	ha4	77-97%	++	++	+++	++	-
ha5	ha5	77-90%	+++	++	++	++	-
ha6	ha6	80-100%	+	+	+++	++	-
hc2	hc2	77-97%	+	-	-	+	-
hc1	hc1	52-62%	+	+	-	+	-
hp1-2	hp1, hp2	36-68%	+	++	-	+	-
ha1	ha1	55-77%	++	-	+	++	-
ha2-3	ha2, ha3	83-97%	++	+	++	+++	-
hp3	hp3	71-90%	+	+	-	++	-
hp4	hp4	68-93%	+	+	++	++	-
pf	pf1, pf2	71-90%	+	++	+	++	-
fl1-2	fl1, fl2	49-74%	+	++	-	+	-
fl3	fl3	71-62%	++	++	+	-	-

fl4	fl4	59-100%	+++	++	++	-	+
fl5	fl5	83-100%	++	+	-	-	-
no1-2	no1, no2	6-29%	++	++	++	+	+++
no3	no3	16-24%	++	+	-	+	-
no4	no4	13-21%	+	+	++	+	-
no5	no5	16-20%	+	+	+	+	-

925

926

927 Correspondence to the definition in Fujita et al. (2012), and location of the cluster
 928 within the caudorostral level of the cerebellum are shown (columns 2,3). Relative
 929 intensity in immunostaining in the present study (columns 4-8) was generally consistent
 930 with the previous result (Fujita et al., 2012), but showed some minor differences. In
 931 cluster names, “v”, “i”, “h”, “a”, “p”, “t”, “c”, “fl”, “no” means vermal, intermediate
 932 (paravermis), hemisphere, anterior, posterior, translobular (anterior+posterior), central,
 933 floccular, nodular, respectively. The numeral (such as “1” in “vp1”) counts the cluster
 934 from the medial to the lateral side in each category (“it1” is absent).

935 Table 4: Changes in the molecular expression profile in PC clusters from E14.5 to E17.5

936

937

E14.5 PC cluster and E17.5 lineage clusters (Definition in Fujita et al. 2012 if it is different)		Changes from E14.5 to E17.5			
		Corl2	Pcdh10	EphA4	FoxP2
m		+ ~ +++	- ~ ++	- ~ +++	+ ~ +++
	vt1	(+)	(++)	(-)	(+)
	vt2	(+++)	>> +	>> +	(++)
	vc1	(+++)	>> +++	(++)	(+++)
	vp1-2 (vp1, vp2)	(++)	>> +	(++)	(+++)
	vt3	>> ++	(+++)	(+)	>> ++
	no1-2 (no1, no2)	>> ++	(++)	(++)	(+++)
d		++	++	-	+++
	vt5		>> +		>> ++
	vt4			>> ++	
	va1				
c-m		+++	++ ~ +++	++	+
	vp3-4 (vp3, vp4, vc2)		>> +	>> +++	
	ic1-2 (ic1, ic2)		(+++)	>> +++	
	ic3		>> -		
	no4	>> ++	>> +		
	no5	>> +	>> +		
	no3	>> +	>> +		
c-l		++	+/-	++	++
	va2-4 (va2, va3, va4)	>> +++	>> -	>> -	
	ip1-2 (ip1, ip2)	>> +	>> -	>> -	
	ia1-2 (ia1, ia2)	>> +	>> -	>> -	
	it3		>> -	>> +++	>> +++
	ha4			>> +++	>> +++
	ia3-5 (ia3, ia5)		>> -	>> +++	> +++
ml		+	+++	+++	+++
	it2 (it2, ic5, ip3)	>> ++		>> -	
	ia4 (ia4, ic4)	> ++	>> +	>> -	

dl		+++	+/-	++	++
	hp1-2 (hp1, hp2)	>> +	>> +	>> -	>> +++
	hc1	>> +		>> -	
	ha1	>> ++	>> -	>> +	
	ha2-3 (ha2, ha3)	>> ++	>> +		
rdl		+++	++	+++	+++
	hp3	>> +	>> +	>> -	>> ++
	hp4	>> +	>> +	>> ++	>> +
	pf (pf1, pf2)	>> +		>> +	
l		++	+	++	++
	ha5	>> +++			
	ha6	>> +		>> +++	
	hc2	>> +	>> -	>> -	
vl		++	+/-	+/-	-
	fl1-2	>> +	>> ++	>> +	
	fl3		>> ++		
	fl4	>> +++	>> ++	>> ++	
	fl5		>> ++	>> ++	

938

939

940 “~” indicates the gradient in the molecular expression intensity.

941 “>>” indicates the change in the molecular expression intensity

942 Table 5: Afferent and efferent connections of the cerebellar modules that were derived
 943 from the c-1 lineage clusters.
 944

E14.5 PC cluster	Birthdate of PCs	E17.5 PC cluster	Adult zebrin stripe(s)	Module	IO ¹⁾	CN ²⁾
c-1	E11.5, E12.5	va2-4	2- (lateral) and b+ in I-V	B	dDAO	LVN
		ip1-2	4-, f+, f-, e1+ in Cop	C1	vDAO lateral	AIN
		ia1-2	b-, 3+ in I-V	C1	vDAO central	AIN
		ia3-5	3-, 3b+, 3b- in III, IV-V	C1	vDAO central	AIN
		it3	4-//5- (medial) in III, IV-V, Sim, Cr I, Cr II,	C3	vDAO medial	AIN

			Par			
		ha4	5- in IV-V	D0	DM	AIN

945

946 1) Inferior olive subarea that project to PCs in the stripe (Sarpong et al., 2018;
 947 Sugihara and Shinoda, 2004).

948 2) Cerebellar nucleus subarea that is innervated by PCs in the stripe (Sugihara et al.,
 949 2009).

950 Abbreviations: I-V, lobules I-V; III, lobule III; IV-V, lobule IV-V; AIN, anterior
 951 interposed nucleus; CN, cerebellar nucleus; Cop, copula pyramidis; Cr I, crus II; Cr II,
 952 crus II; dDAO, dorsal fold of the dorsal accessory olive; DM dorsomedial subnucleus;
 953 IO, inferior olive; LVN, lateral vestibular nucleus; Par, paramedian lobule; Sim, simple
 954 lobule; vDAO, ventral fold of the dorsal accessory olive.

955

956 Figure 1. Introductory schematic drawings of the somatotopy and compartments
957 mapped in the unfolded scheme of the mouse cerebellar cortex. A, Somatotopy mainly
958 based on mapping of mossy fiber terminal response (Welker, 1987) and labeled
959 spinocerebellar and cuneocerebellar projections in rodents (Quy et al., 2011; Luo et al.,
960 2018, 2020). B, Olivocorticonuclear modules (colored areas) defined by the topographic
961 axonal projections between subareas of the inferior olive, cerebellar nuclei and
962 cerebellar cortex (A, AX, A2, B, CX, X, X-CX, C1, C2, C3, D0, D1 and D2 modules;
963 Voogd and Glickstein, 1993; Sugihara and Shinoda, 2004; Ruigrok et al., 2015).
964 Shadowed areas belong to aldolase C-positive stripes. C, Stripes defined by aldolase C
965 expression pattern in Purkinje cells (Fujita et al., 2014; Sarpong et al., 2019). D and E,
966 Mapping of clusters of PCs at E14.5 and immature stripes of PCs at P6 based on Fujita
967 et al. (2012). Blue areas indicate particular clusters or immature stripes that express lacZ
968 in 1NM13 transgenic mice, which often overlap with zebrin stripes. Abbreviations, c-l,
969 c-m, d, dl, l, m, ml, rdl, vl, names of E14.5 clusters; C, caudal; D, dorsal; L, lateral; M,
970 medial; R, rostral. V, ventral.

971

972 Figure 2. Purkinje cell clusters in coronal sections of the left E14.5 mouse cerebellum
973 identified by marker expression profiles. A–E, Sections at different caudorostral levels
974 indicated by percentile. Fluorescent signals of immunostaining for Corl 2 (red), Pcdh10
975 (blue) and FoxP2 (green) are merged. Inset in each panel shows drawings of recognized
976 clusters at half magnification. Squares indicate areas that are magnified. F–H,
977 Magnified images showing PC-free gaps (arrowheads) between some clusters. I, Dorsal
978 view of the 3D reconstruction of clusters. Red lines indicate the rostrocaudal level of the
979 section in each panel. Scale bar in E (100 μ m) applies to A–E. Scale bar in F (100 μ m)
980 applies to F–H. Abbreviations, c-l, c-m, d, dl, l, m, ml, rdl, vl, names of E14.5 clusters;
981 C, caudal; D, dorsal; L, lateral; M, medial; R, rostral. V, ventral.

982

983

984 Figure 3. Purkinje cell clusters in coronal sections of the left E15.5 mouse cerebellum
985 identified by marker expression profiles. A–G, Sections at different caudorostral levels
986 indicated by percentile. Fluorescent signals of immunostaining for Corl 2 (red), Pcdh10
987 (blue) and FoxP2 (green) are merged. Inset in each panel shows drawings of recognized
988 clusters at half magnification. Names of each cluster were given later based on the
989 lineage analysis (c.f. Fig. 7). H, Dorsal view of the 3D reconstruction of clusters. Red
990 lines indicate the rostrocaudal level of the section in each panel. Scale bar in G (100
991 μm) applies to panels A–G. Abbreviations, c-l, c-m, d, dl, l, m, ml, rdl, vl, names of the
992 lineage of clusters; C, caudal; D, dorsal; L, lateral; M, medial; R, rostral. V, ventral.

993

994 Figure 4. Purkinje cell clusters in coronal sections of the left E16.5 mouse cerebellum
995 identified by marker expression profiles. A–I, Sections at different caudorostral levels
996 indicated by percentile. Fluorescent signals of immunostaining for EphA4 (red), Pcdh10
997 (blue) and FoxP2 (green) are merged. Inset in each panel shows drawings of recognized
998 clusters at half magnification. Names of each cluster were given later based on the
999 lineage analysis (c.f. Fig. 7). J, Dorsal view of the 3D reconstruction of clusters. Red
1000 lines indicate the rostrocaudal level of the section in each panel. Scale bar in A (100 μm)
1001 applies to panels A–I. Abbreviations, c-l, c-m, d, dl, l, m, ml, rdl, vl, names of the
1002 lineage of clusters; C, caudal; D, dorsal; L, lateral; M, medial; R, rostral. V, ventral.

1003

1004 Figure 5. Purkinje cell clusters in coronal sections of the left E17.5 mouse cerebellum
1005 identified by marker expression profiles. A–I, Sections at different caudorostral levels
1006 indicated by percentile. Fluorescent signals of immunostaining for EphA4 (red), Pcdh10
1007 (blue) and FoxP2 (green) are merged. Inset in each panel shows drawings of recognized
1008 clusters at half magnification. Names of each cluster were adopted from Fujita et al.
1009 (2012). J, Dorsal view of the 3D reconstruction of clusters. Yellow lines indicate
1010 immature fissures. Red lines indicate the rostrocaudal level of the section in each panel.
1011 Scale bar in A (100 μm) applies to panels A–I. Abbreviations, hc2, ha6, hp4, hc1, ha2,
1012 ha4, hp2,it3, it2, ia4, ia1-2, ic3, ip1-2, ic1-2, va2-4, vp3-4, va1, vt5, vt4, vt3, vt2, vt1,
1013 vc1, vp1-2, names of E17.5 clusters; C, caudal; D, dorsal; L, lateral; M, medial; R,
1014 rostral. V, ventral.

1015

1016 Figure 6. Spatial distribution of E10.5-, E11.5-, and E12.5-born PCs in the E14.5
1017 cerebellum. A–D, Images of coronal sections of the left cerebellum of G2A::Ai9
1018 embryos which had tamoxifen injection at E10.5 (subpanel 1), E11.5 (subpanel 2) and

1019 E12.5 (subpanel 3) at different rostrocaudal levels. The top, center and bottom panels
1020 show images of the tdTomato fluorescence signal (top), three signals merged, and
1021 signals of tdTomato fluorescence (green) and immunostaining signals of Pcd10 (red)
1022 and EphA4 (blue) in (A), while only the tdTomato fluorescence signal is shown in (B–
1023 D). The tdTomato signal indicates neurons (mostly PCs) that expressed *Neurog2*-CreER
1024 at the time of tamoxifen injection. Subpanel 4 shows schematic drawings of identified
1025 clusters. Blue and Orange asterisks indicate (position of) the E10.5-PC-sparse and
1026 E12.5-PC-sparse clusters, respectively. E, Relative labeling density in nine E14.5
1027 clusters. The plotted data were the average of the tdTomato fluorescence signal in the
1028 digital file (0-255) measured in 9-18 square areas of $900\ \mu\text{m}^2$ located inside the
1029 identified cluster in 3-6 sections. The same brightness and contrast adjustment was done
1030 in all sections. F, Confocal high-magnification image of immunostaining and tdTomato
1031 expression at the junction between the ml and c-l clusters in the AM10.5 G2A::Ai9
1032 embryo, showing expression of tdTomato (E10.5-born neurons) colocalized exactly
1033 with Corl2 (PC marker) at the cellular level in the ml cluster. The area of this image is
1034 indicated in (C2) with a square. Abbreviations, c-l, c-m, d, dl, l, m, ml, rdl, vl, names of
1035 E14.5 clusters; C, caudal; D, dorsal; L, lateral; M, medial; R, rostral. V, ventral.

1036

1037 Figure 7. Identification of TM10.5 PC-free and TM12.5 PC-free clusters in the
1038 E14.5-E17.5 cerebellums. A–D, Images of coronal sections of the TM10.5 and TM12.5
1039 cerebellums at nearly the same level (subpanel 1 and 2, respectively) and schematic
1040 drawing of clusters (subpanel 3) and dorsal view of the 3D scheme (subpanel 4) of the
1041 E14.5 (A), E15.5 (B), E16.5 (C), and E17.5 (D) cerebellums. In subpanels 1 and 2, the
1042 tdTomato fluorescence signal (top), three signals merged, and signals of tdTomato
1043 fluorescence (green) and immunostaining signals of Pcd10 (red) and EphA4 (blue) are
1044 shown from the top to the bottom. Blue and orange colors in dashed lines (in subpanels
1045 in 1 and 2), circumscribing lines (in subpanels 3), and clusters in the 3D schemes (in
1046 subpanels 4) indicate TM10.5 PC-free and TM12.5 PC-free clusters. Black line in the
1047 3D scheme indicates the position of the coronal section in subpanels 1-3. Abbreviations,
1048 c-l, c-m, d, dl, l, m, ml, rdl, vl, names of E14.5 clusters; hc2, ha6, hp4, hc1, ha2, ha4,
1049 hp2, it3, it2, ia4, ia1-2, ic3, ip1-2, ic1-2, va2-4, vp3-4, va1, vt5, vt4, vt3, vt2, vt1, vc1,
1050 vp1-2, names of E17.5 clusters; C, caudal; D, dorsal; L, lateral; M, medial; R, rostral. V,
1051 ventral.

1052

1053 Figure 8. Separated distribution of the E10.5-PC-sparse c-l lineage clusters in the E17.5
1054 cerebellum. A–F, Images of a part of the coronal section at various rostrocaudal levels

1055 of the left cerebellum. The top subpanel shows the merged signal of Pcdh10
 1056 immunostaining (red), EphA4 immunostaining (blue) and tdTomato expression
 1057 indicating E10.5-born PCs (green), whereas the bottom subpanel shows only tdTomato
 1058 expression. Scale bar in F applies A–F. G, Dorsal view of the 3D scheme of the c-l
 1059 lineage clusters in the left E17.5 cerebellum, compared with the single c-l cluster in the
 1060 left E14.5 cerebellum. Abbreviations, ha4, it3, ia1-2, ip1-2, va2-4, names of E17.5
 1061 clusters; C, caudal; D, dorsal; L, lateral; M, medial; R, rostral.V, ventral.

1062

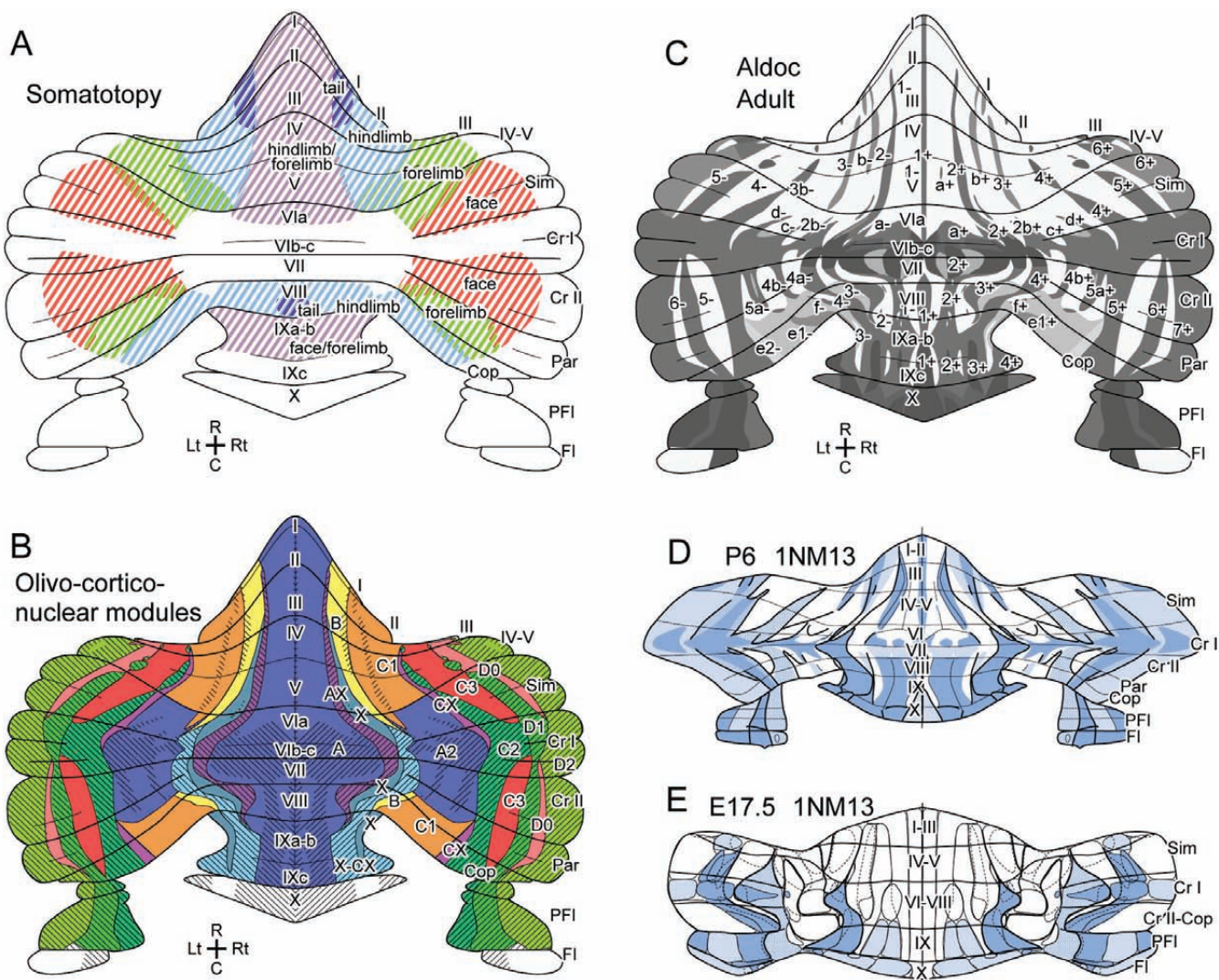
1063 Figure 9. Separation and migration of the c-l lineage cluster from E14.5 to E17.5. A,
 1064 Horizontal sections of the left paravermal and hemispheric cerebellum at around the
 1065 central level. Sections were immunostained for Corl2 (green channel), EphA4 (blue
 1066 channel), and Pcdh10 (red channel). Dashed lines circumscribe c-l lineage clusters.
 1067 Arrowheads indicate the lateral migration of the rostral c-l lineage clusters. B, Dorsal
 1068 view of the three-dimensional scheme of reconstructed c-l lineage clusters (blue). In the
 1069 bottom panel, ml and c-m lineage clusters (orange and white) are added. C, Images of a
 1070 part of the left cerebellum at the junction between the c-l and c-m lineage clusters in
 1071 coronal sections. The top image shows merged signals of tdTomato expression, which
 1072 indicates E10.5-born PCs (green) and immunostaining for EphA4 (blue) and Pcdh10
 1073 (red). The bottom subpanel shows only the image of only tdTomato labeling. D,
 1074 Schematic drawing of clusters shown in (C). In (A–D), columns of subpanels 1-4 are
 1075 from E14.5, E15.5, E16.5 and E17.5 cerebellums. Dashed lines indicate c-l lineage
 1076 clusters that were mostly devoid of E10.5-born PCs and weak in Pcdh10 expression in
 1077 (A and C). Single asterisks indicate the most medial portion of the c-l lineage clusters
 1078 that had higher expression of Corl2 than the rest of the c-l lineage cluster in (A–D).
 1079 Double asterisks indicate the lateral part of the c-m lineage cluster that intercalated the
 1080 c-l lineage clusters in (A–D). Arrows indicate the direction of cluster migration. Scale
 1081 bar in C1 (100 μ m) applies to C1–C4. Abbreviations, c-l, c-m, d, ml, names of E14.5
 1082 clusters; hc2, ha6, hp4, hc1, ha2, ha4, hp2,it3, it2, ia4, ia1-2, ic3, ip1-2, ic1-2, va2-4,
 1083 vp3-4, va1, vt5, vt4, vt3, vt2, vt1, vc1, vp1-2, names of E17.5 clusters; C, caudal; D,
 1084 dorsal; L, lateral; M, medial; R, rostral.V, ventral.

1085

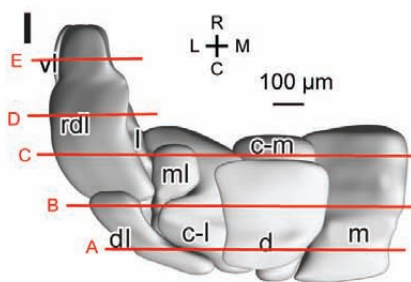
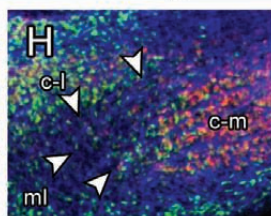
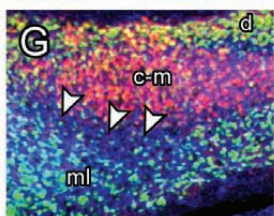
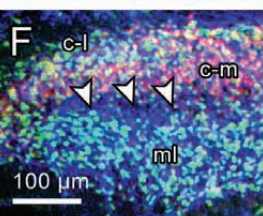
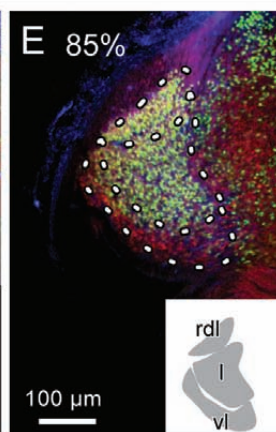
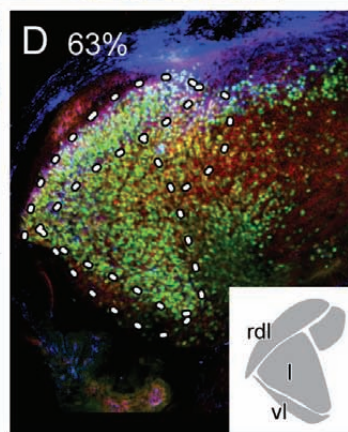
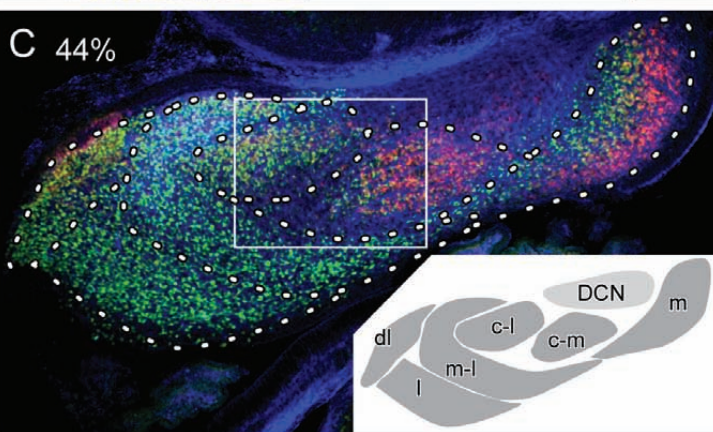
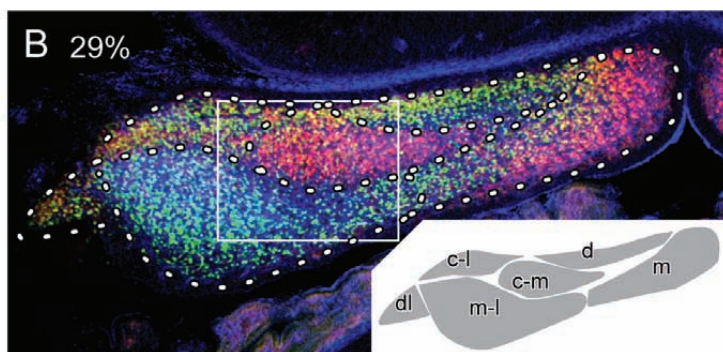
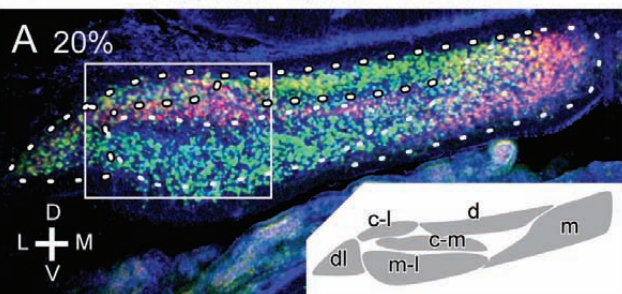
1086 Figure 10. The fate of c-l lineage clusters in the compartmentalization of the adult
 1087 cerebellar cortex. A, Confocal high magnification images of the cerebellar cortex of the
 1088 G2A::Ai9::AldocV mouse in which tamoxifen was given at E11.5, showing tdTomato
 1089 expression in Purkinje cells. B, Four coronal sections of the left cerebellum at rostral
 1090 (B1), central (B2) and caudal (B3, B4) levels in the G2A::Ai9::AldocV mouse that

1091 received tamoxifen at E10.5 and sacrificed at P42. Superimposed images of magenta
1092 (tdTomato representing E10.5-born PCs) and green (Venus representing aldolase C
1093 expression) channels are shown in the left, while only green channel (Venus, aldolase C)
1094 is shown in the right. E10.5-PC-sparse areas that were considered to belong to the
1095 lineage of the c-l cluster were circumscribed by yellow lines. Arrowheads indicated
1096 labeled PC somata that were observed within the circumscribed area. Zebrin stripes
1097 were indicated in the right panels. Scale bar (500 μ m) applies to B1-B4. Inset in panel
1098 B1 shows sparse Purkinje cell labeling at the dendrite (left) and at the soma and dendrite
1099 (arrowhead) in the c-l lineage area. C, Schematic of intermittent PC generation in the
1100 ventricular zone of the left embryonic cerebellum. D, Schematic of the c-l cluster
1101 composed of randomly located E11.5- and 12.5-born PCs in the left E14.5 cerebellum.
1102 E, Schematic of separation and migration of c-l lineage clusters (blue, green and red) at
1103 E17.5. Gray clusters are non-c-l-lineage clusters that separate the green clusters into the
1104 anterior and posterior parts and separate the blue cluster into the anterior and posterior
1105 parts later. F, Mapping of the E10.5-PC-sparse areas that were considered to belong to
1106 the lineage of the c-l cluster mapped the unfolded scheme of the entire cerebellar cortex
1107 with the zebrin striped pattern (Sarpong et al., 2018). Projections of the B module and
1108 C1/C3/D0 modules are shown schematically. Abbreviations: 1+, 1- and so on, aldolase
1109 C (zebrin) stripes 1+, 1- and so on; I-X, lobules I-X; a-c, sublobules a-c (as in IXa-b);
1110 AIN, anterior interposed nucleus; B, C1, C3, D: modules B, C1, C3 and D0; C, caudal;
1111 Cop, copula pyramidis; Cr I, crus I; Cr II, crus II; D, dorsal; Fl, flocculus; ha4, ia1-2,
1112 ia3-5, ic1-2, ip1-2, it2, it3, oc3, va2-4 names of E17.5 PC clusters; L, lateral; LVN,
1113 lateral vestibular nucleus; M, medial; M1, primary motor cortex; Par, paramedian
1114 lobule; PFl, paraflocculus; R, rostral; Sim, simple lobule; V, ventral.

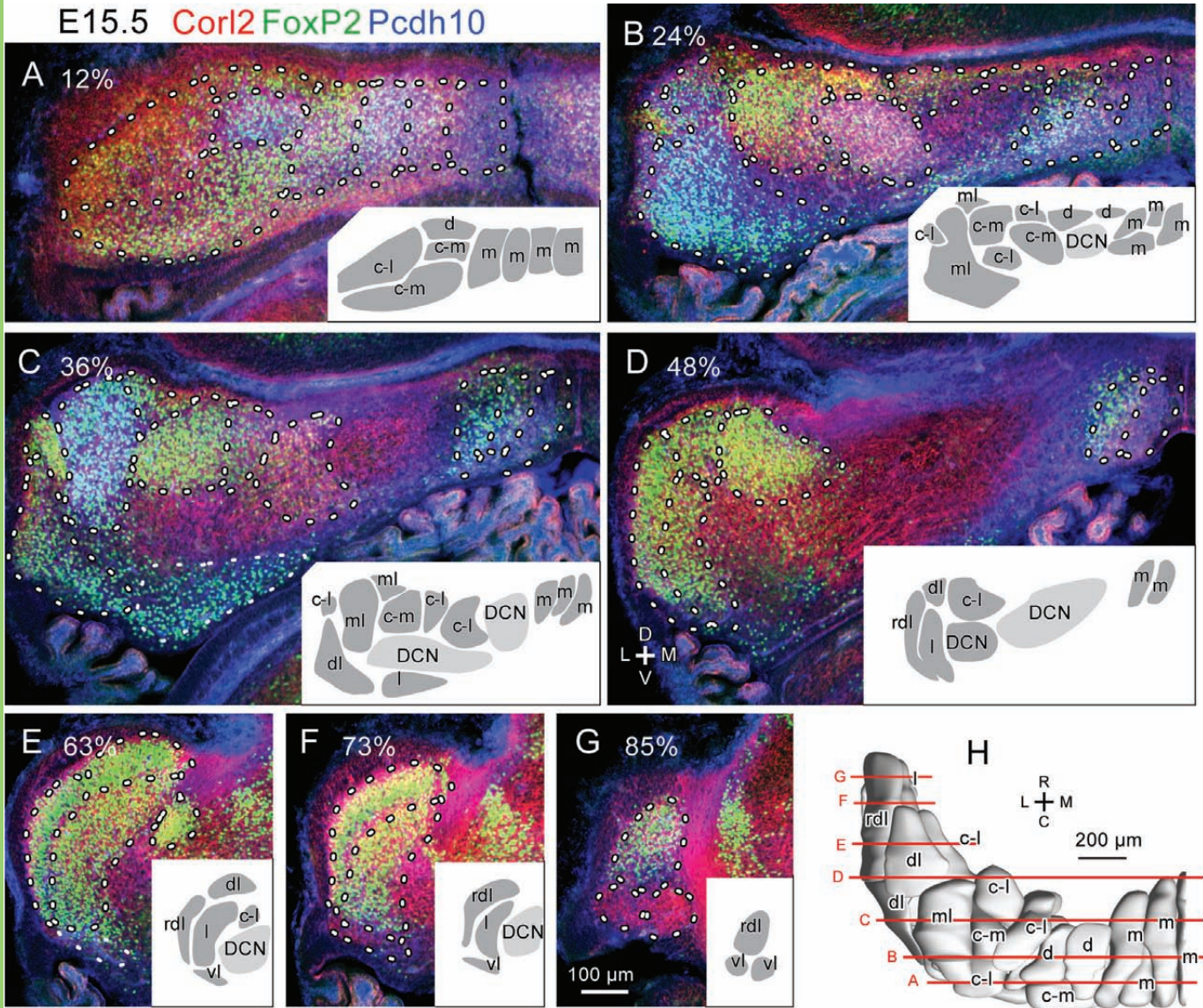
1115
1116
1117
1118
1119
1120
1121
1122
1123



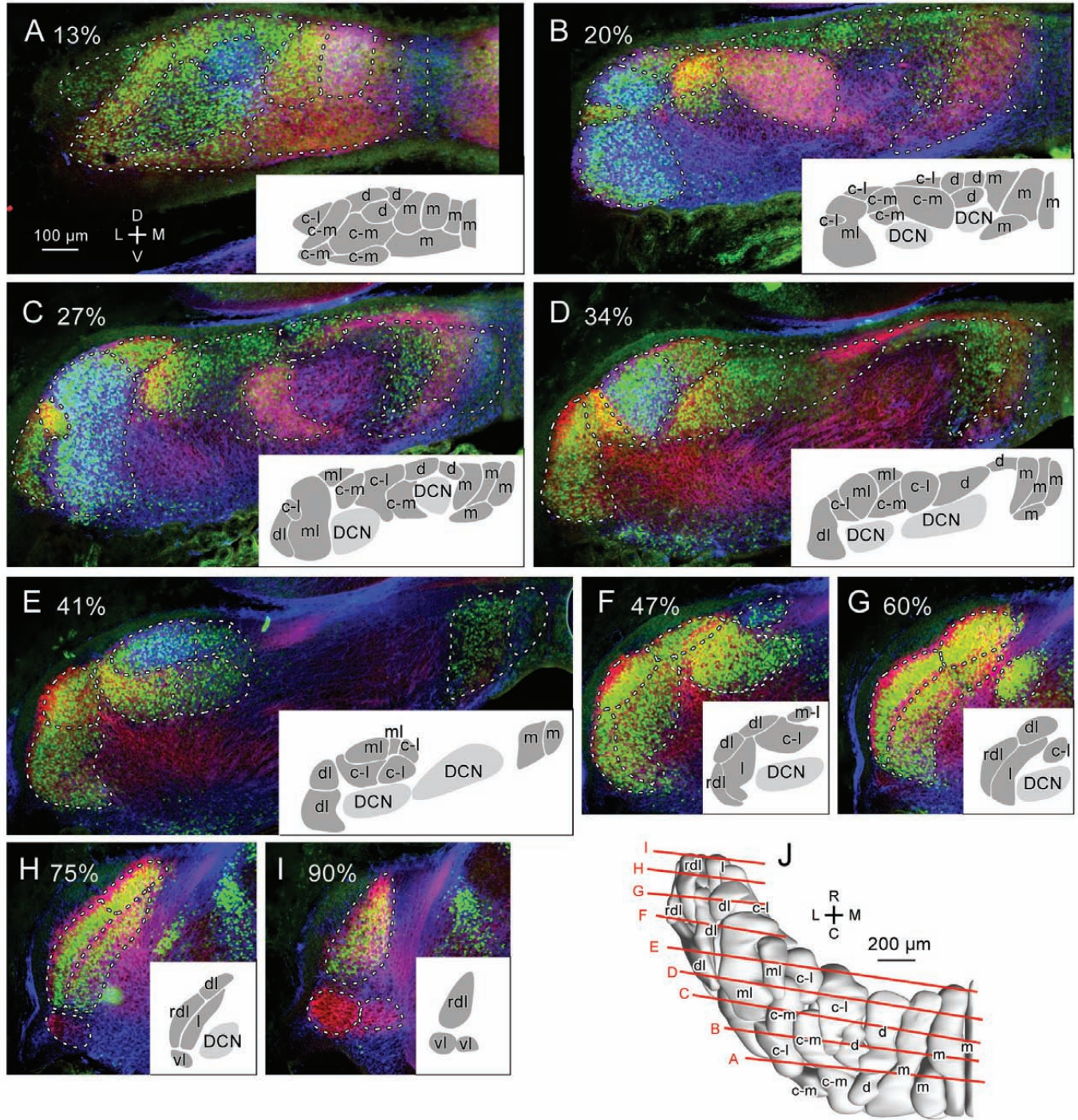
E14.5 **Corl2** **FoxP2** **Pcdh10**



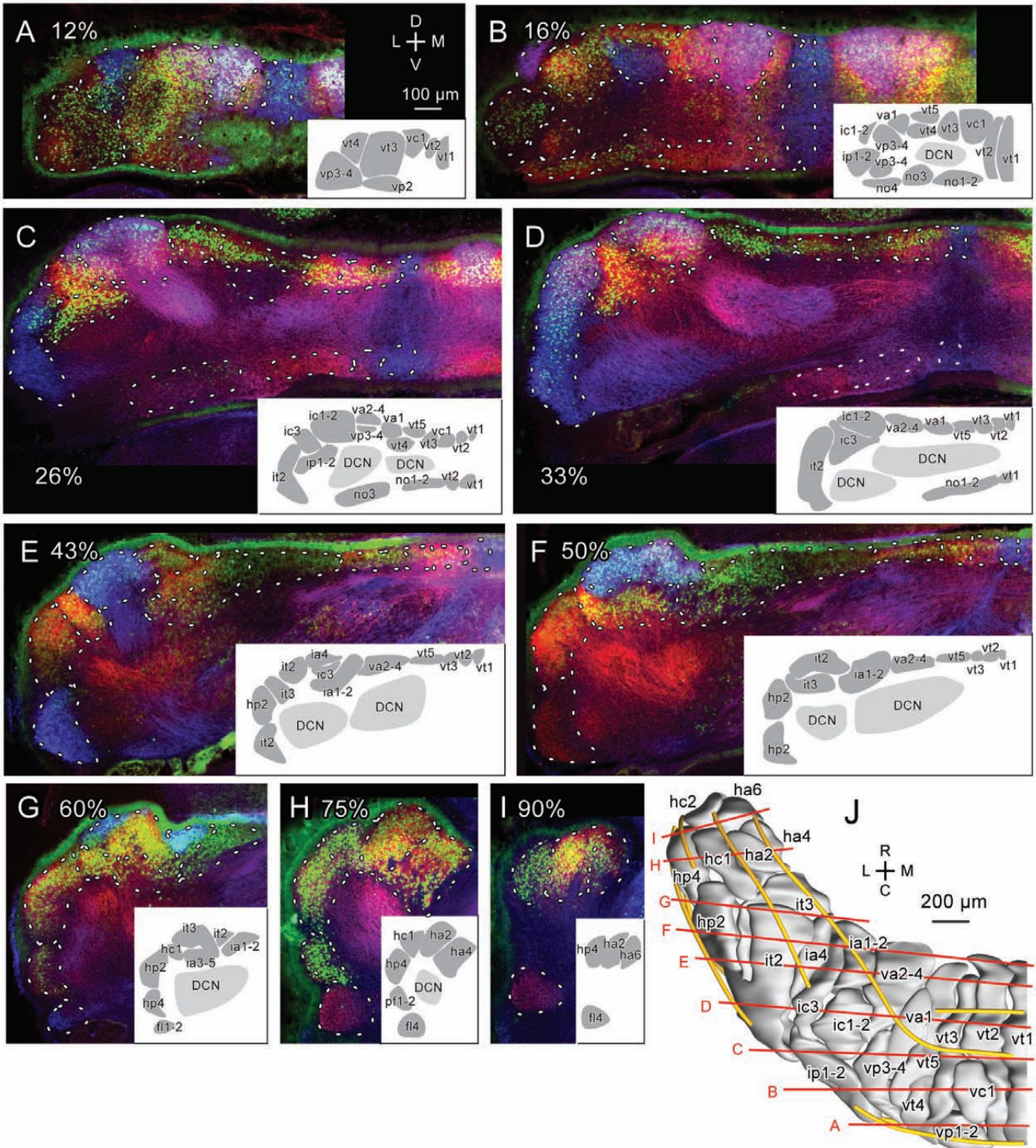
E15.5 Corl2 FoxP2 Pcdh10

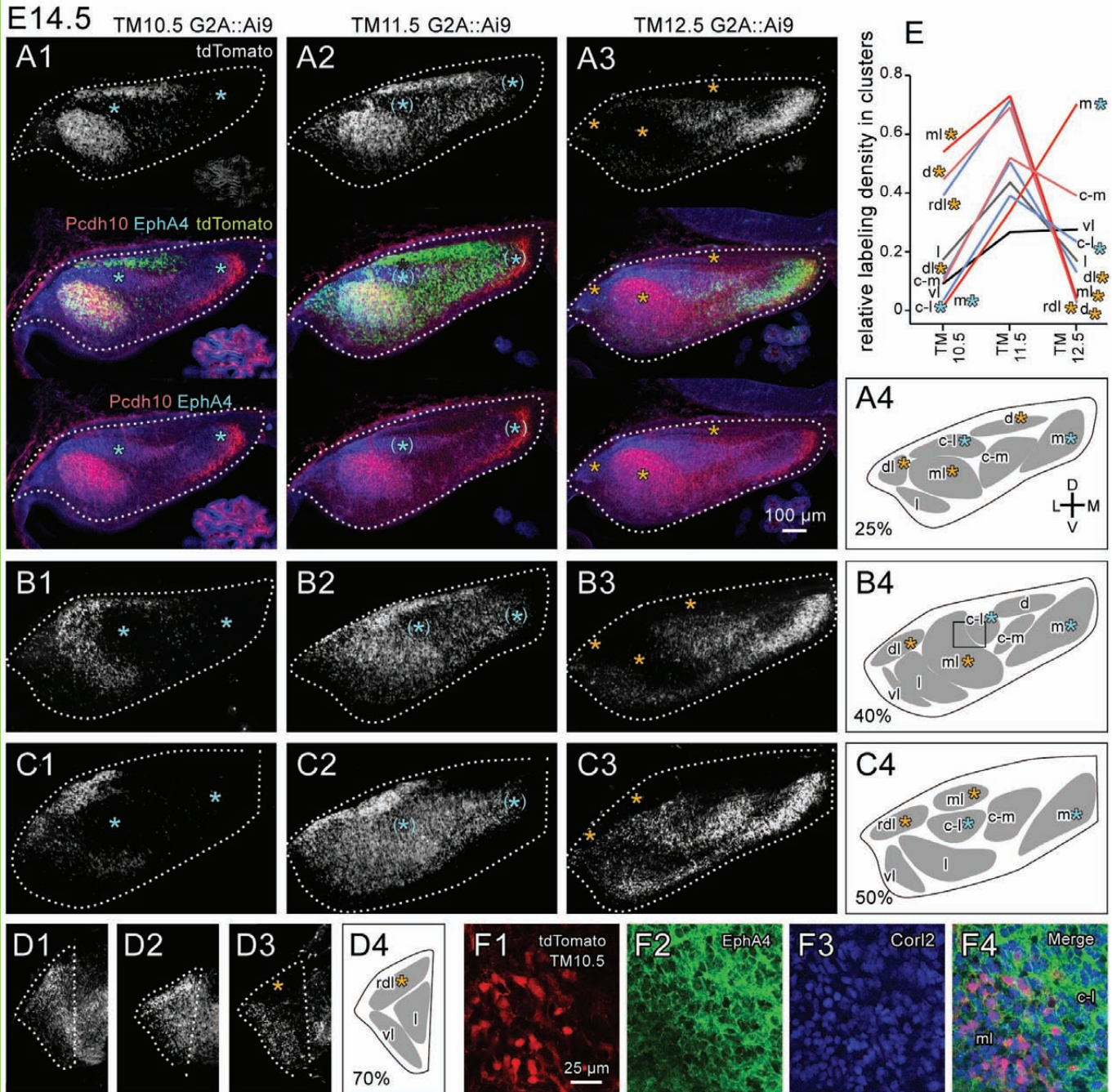


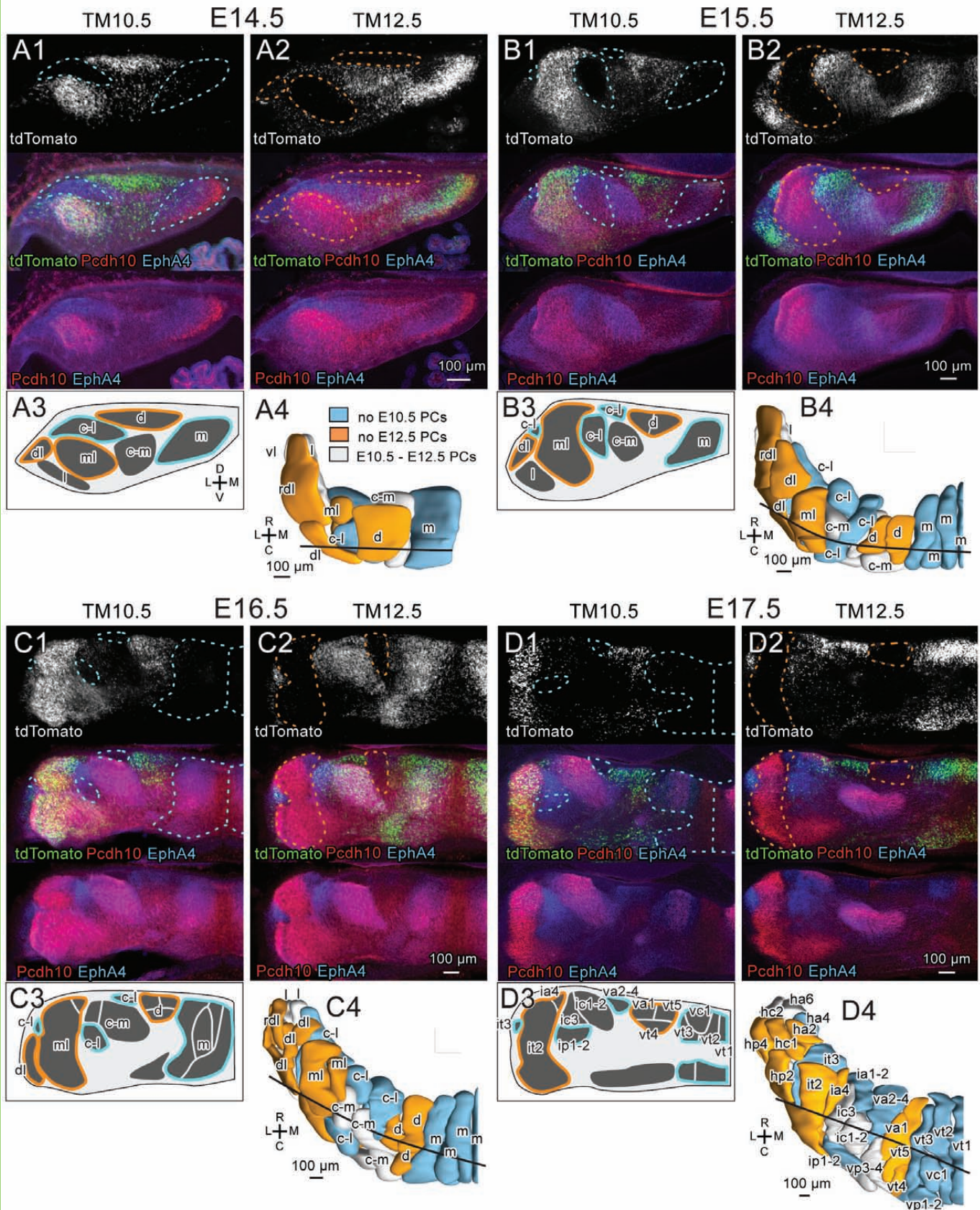
E16.5 EphA4 FoxP2 Pcdh10



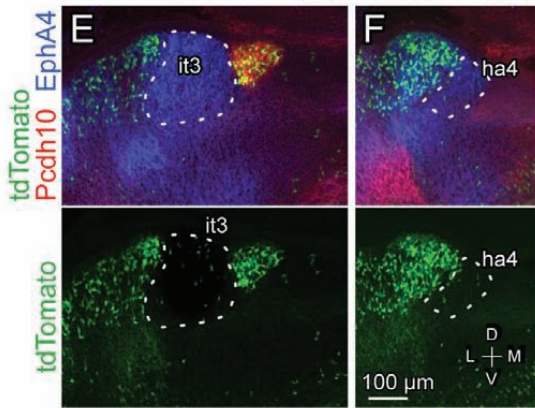
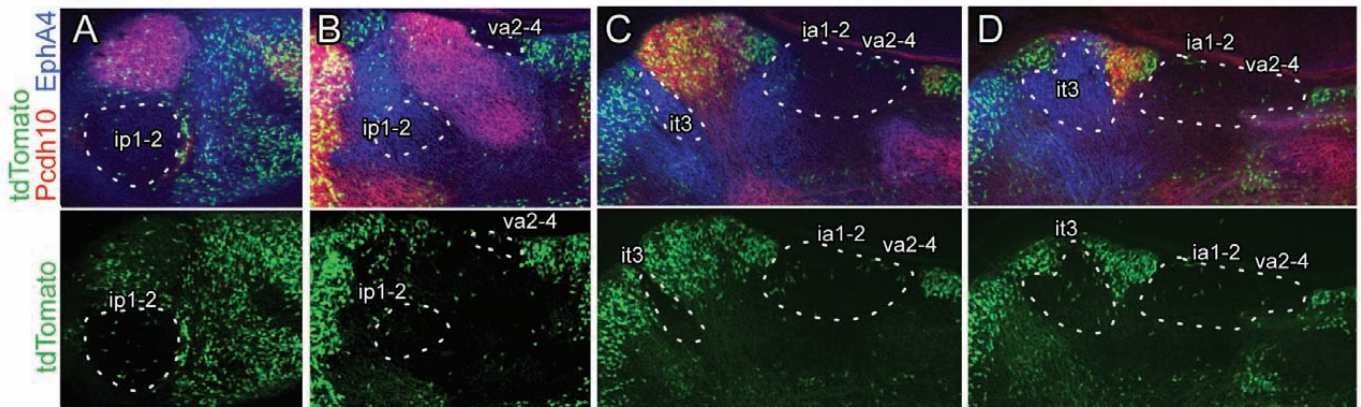
E17.5 EphA4FoxP2Pcdh10







E17.5 TM10.5



G c-l lineage clusters that nearly lack TM10.5 PCs

